ATION PAGE

Form Approved
OMB No 0704-0188

1. AGENCY USE ONLY (Leave blank)	2. REPORT DATE	3. REPORT TYPE AND DATES COVERED
	3/3/92	Final Technical Rep. 10/1/88 - 9/30/91

4. TITLE AND SUBTITLE
A Combined Experimental and Analytical Investigation of the Theory of Plasticity Involving Strain-Induced Anisotropy

5. FUNDING NUMBERS

6. AUTHOR(S)
E.H. Lee, E. Krempl and T.L. Sham

7. PERFORMING ORGANIZATION NAME(S) AND ADDRESS(ES)
Erastus H. Lee and Erhard Krempl, P.I.'s
Dept. of Mechanical Eng., Aero. Eng. and Mechanics
Rensselaer Polytechnic Institute, Troy, NY 12180-3590

8. PERFORMING ORGANIZATION REPORT NUMBER

9. SPONSORING/MONITORING AGENCY NAME(S) AND ADDRESS(ES)
U. S. Army Research Office
P. O. Box 12211
Research Triangle Park, NC 27709-2211

10. SPONSORING/MONITORING AGENCY REPORT NUMBER

11. SUPPLEMENTARY NOTES
The view, opinions and/or findings contained in this report are those of the author(s) and should not be construed as an official Department of the Army position, policy, or decision, unless so designated by other documentation.

12a. DISTRIBUTION/AVAILABILITY STATEMENT
Approved for public release; distribution unlimited.

12b. DISTRIBUTION CODE

13. ABSTRACT *(Maximum 200 words)*

Experiments were carried out which subjected tubes of ductile metals to histories of straining in combined tension/compression/torsion space. The computer controlled servo-hydraulic testing machine recorded the resulting stress histories together with the imposed strain histories. Intermittently along the path, the straining was halted to probe for the current yield locus. The nose of the yield locus in the direction of straining exhibited quite accurately a circular geometry, which implied isotropic-kinematic hardening.

The centers of the fitted yield circles in $(\sigma, \sqrt{3}\,\tau)$ generalized tension-shear space, define the back stress α which expresses the anisotropic component of the hardening. α expresses the strength and orientation of the impediment to dislocation flow through the crystal, i.e. the yield stress required to maintain plastic flow. Application of a polygonal closed straining path caused the back stress tensor to rotate about 330° while the material rotation due to shear was only about 1°. Thus plastic spin, which in the literature has been considered to cause spin of the plastic anisotropy, turns out to be very much smaller.

Measurements of stress response to linear and nonlinear strain paths have been used to generate the evolution law for the back stress and hence the constitutive relation.

14. SUBJECT TERMS
Plastic strain-induced anisotropy, isotropic-kinematic-hardening, evolution of back stress

15. NUMBER OF PAGES
43

16. PRICE CODE

17. SECURITY CLASSIFICATION OF REPORT	18. SECURITY CLASSIFICATION OF THIS PAGE	19. SECURITY CLASSIFICATION OF ABSTRACT	20. LIMITATION OF ABSTRACT
UNCLASSIFIED	UNCLASSIFIED	UNCLASSIFIED	UL

A COMBINED EXPERIMENTAL AND ANALYTICAL INVESTIGATION OF THE THEORY OF PLASTICITY INVOLVING STRAIN INDUCED ANISOTROPY

FINAL REPORT

E.H. LEE, E. KREMPL AND T.-L. SHAM

March 3, 1992

U.S. ARMY RESEARCH OFFICE

CONTRACT NO. DAAL03-88-K-0041

Department of Mechanical Engineering,
Aeronautical Engineering & Mechanics
Rensselaer Polytechnic Institute
Troy, New York 12180-3590

THE VIEW, OPINIONS, AND/OR FINDINGS CONTAINED IN THIS REPORT ARE THOSE OF THE AUTHORS AND SHOULD NOT BE CONSTRUED AS AN OFFICIAL DEPARTMENT OF THE ARMY POSITION, POLICY, OR DECISION, UNLESS SO DESIGNATED BY OTHER DOCUMENTATION.

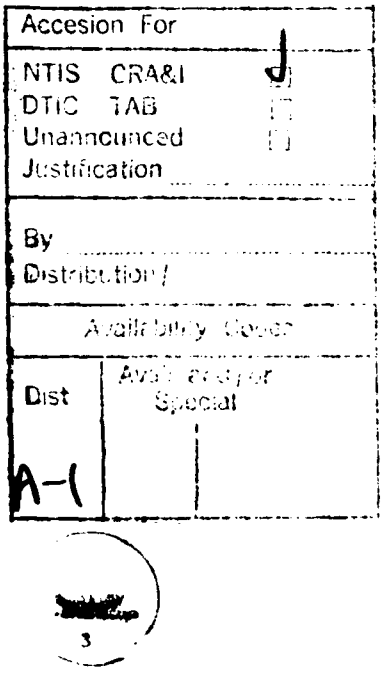

Table of Contents

List of Figures ..... (i)

Introduction 1

The Testing Program for Material Characteristics 2

The Structure of the Constitutive Relation 5

Determination of the Constitutive Relation 7

Conclusions 11

Figures 13

List of Publications 34

List of Participating Scientific Personnel 37

LIST OF FIGURES

Figure 1 Strain controlled tension test with intermittent unloading and re-loading

Figure 2 Stress controlled tension test with intermittent unloading and re-loading

Figure 3 Sequence of 16 excursions used to determine the stresses and strains at the onset of renewed plasticity

Figure 4 An example of the yield locus probing procedure

Figure 5 The prescribed strain history of the polygonal and square paths

Figure 6a Yield surface measurement for station 6. The center of the fitted circle is related to the back stress α.

Figure 6b Yield surface measurement for station 14. The center of the fitted circle is related to the back stress α.

Figure 7 Strain generated by unloading from a tension test followed by re-loading in tension or compression

Figure 8 Evolution of the backstress α for the polygonal path

Figure 9a Prescribed nonproportional straining path 34g1

Figure 9b Prescribed proportional straining path 34g2

Figure 9c Prescribed proportional straining path 34g3

Figure 9d Prescribed nonproportional straining path 34f3

Figure 10a Recorded stress response from nonproportional straining path 34g1

Figure 10b Recorded stress response from proportional straining path 34g2

Figure 10c Recorded stress response from proportional straining path 34g3

Figure 10d Recorded stress response from nonproportional straining path 34f3

Figure 11a Axial stress versus $\bar{\varepsilon}^p$ from the proportional straining path 34g2

Figure 11a Shear stress versus $\bar{\varepsilon}^p$ from the proportional straining path 34g2

Figure 12 Trajectories of the centers of the circular yield loci in the (σ, $\sqrt{3}\,\tau$) space

Figure 13 The function η_1 plotted as a function of $\bar{\alpha}$ for all four straining paths. The function η_1 is obtained from the evolution equations by setting η_2 and η_3 to zero. Least-squares method was employed in extracting η_1 from three scalar evolution equations.

A COMBINED EXPERIMENTAL AND ANALYTICAL INVESTIGATION OF THE THEORY OF PLASTICITY INVOLVING STRAIN INDUCED ANISOTROPY

1. Introduction

When plastic flow occurs in the manufacture of machine components or structures, or is anticipated to occur in the use of them or in associated strength and reliability design calculations, isotropic plasticity theory has commonly been adopted because reliable anisotropic theory and the needed material characteristics are not usually available. However, the strain-hardening generated by plastic flow commonly produces anisotropic yield surfaces and hence anisotropic flow laws governing subsequent plastic flow. The restriction to isotropic theory clearly leads to errors in the prediction of the stresses generated by the plastic straining imposed and hence prevents reliable design of the manufacturing process and prediction of characteristics of the product, such as high localized strain concentrations. Experiments were therefore carried out on ductile metals at ambient temperatures to investigate the stresses and yield surfaces generated following imposed histories of strain in tension/compression-torsion space. These are needed to develop appropriate constitutive relations. In order to generalize the results to three-dimensional theory, an additional measurement of the varying diameter of the tube to give the history of circumferential strain was also necessary.

The experiments were carried out by imposing prescribed linear and nonlinear tension/compression-torsion strain paths on tubular specimens using a servo-controlled MTS testing machine. The straining was interrupted intermittently to probe for the yield loci in tension/compression-shear stress-space. The whole process was controlled by a computer without the need for human intervention. Similarly, the vast amount of recorded data, such as the points delineating the yield loci, were plotted automatically from the computer output and interpreted in terms of constitutive theory by the computer without the intervention of human judgement.

2. The Testing Program for Material Characteristics

Pure aluminum, aluminum-magnesium and aluminum-manganese alloys were adopted as examples of ductile metals which exhibit elastic-plastic, essentially rate-independent, material behavior, conforming with classical, strain hardening, elastic-plastic theory. The response to a *strain* controlled tension test with intermittent unloading is shown in Figure 1. It is seen to express elastic-plastic behavior with an extensive range of strain hardening. It exhibits an intergranular instability process known as the Portevin-le Chattalier Effect, but with strain control this does not contribute a sufficient disturbance to prevent application of classical elastic-plastic theory. The unloading and re-loading exhibit reversible elastic behavior. Figure 2 illustrates tension test results under *stress* control in which the instability is much more marked, because, when plastic flow is intermittently re-initiated, the strain rate must jump to very large values instantaneously because the prescribed stress rate remains constant, and as the tangent modulus falls to the small plastic modulus the plastic strain rate must increase suddenly which cannot be precisely accommodated by the servo-drive. In contrast, under strain control the very rapid reduction to the plastic modulus demands only that the stress remains nearly constant and so the stress rate drops suddenly which poses no problem for the servo-drive and the material response. Strain control was used throughout the testing program in order to avoid these instabilities, and this is in conformity with the development of elastic-plastic constitutive relations in which the stress history is expressed in terms of the history of deformation.

In order to interpret tension-torsion testing, it is convenient to utilize the generalized shear stress $\sqrt{3}\,\tau$, where τ is the shear stress and correspondingly the generalized plastic shear strain $\gamma^p / \sqrt{3}$. The Mises J_2 yield condition then becomes

$$\sigma^2 + 3\tau^2 = Y^2 = \sigma^2 + (\sqrt{3}\,\tau)^2 \tag{2.1}$$

and the corresponding plastic work rate

$$\sigma\,\dot{\varepsilon}^p + \tau\,\dot{\gamma}^p = \sigma\,\dot{\varepsilon}^p + \sqrt{3}\,\tau\,(\dot{\gamma}^p / \sqrt{3})\,. \tag{2.2}$$

The Mises yield condition is thus a circle in ($\sigma, \sqrt{3}\,\tau$) space and the corresponding maximum plastic work concept demands normality of the strain rate vector ($\dot{\varepsilon}^p$, $\dot{\gamma}^p$ / $\sqrt{3}$) to the circular yield locus in (σ , $\sqrt{3}\tau$) space.

The first tension/compression-torsion straining test carried out followed a polygonal path in (ε , $\gamma / \sqrt{3}$) space. Probes for yield loci were carried out at each vertex. Figure 3 illustrates the procedure for probing for the yield locus of the material at L_i, the i^{th} vertex or loading point station. The straining path has been linear from the station L_{i-1}. On reaching L_i, the straining is reversed and elastic recovery takes place to the base point B_i inside the current yield locus. A sequence of sixteen excursions from B_i are programmed in the numerical order shown in Figure 3 to determine the stresses and strains at the onset of renewed plasticity, that is at points on the new yield locus following deformation along L_{i-1} – L_i. Along each excursion the controlling computer records the strains and stresses at fourteen points planned to remain within the current elastic region and carries out a least-squares fit for straight lines through both axial stress-axial strain and shear stress-shear strain values recorded in the computer. The plot for the axial components of the eleventh excursion are shown in Figure 4. The linear excursion continues in strain space and the computer compares the stress-strain evaluation for both axial and shear components with the linear extension of the fitted elastic lines. The strain deviations thus revealed, $\Delta\varepsilon$ and $\Delta\gamma / \sqrt{3}$, express the renewed plastic flow being initiated. An offset of 10^{-4} was selected to define that a point on the new yield locus had been reached according to

$$\sqrt{(\Delta\varepsilon)^2 + (\Delta\gamma / \sqrt{3})^2} = 10^{-4} . \qquad (2.3)$$

This offset magnitude was chosen to avoid adding appreciable strain hardening from the probing procedure while maintaining a sufficiently definite signal of renewed plastic flow to define a reliable yield locus. For material in the state associated with loading to the strain point L_i, the probing was repeated for each of the sixteen excursions indicated in Figure 3 before continuing the program of plastic straining to the next loading station. Figure 5 shows the total strain history to which this specimen was subjected. Some station numbers are

indicated. The initial deformation from station 1 to station 2 was simple tension followed by a sixteen sided regular polygonal path with yield locus probing at each vertex. Finally a square path was followed. In some cases some station strain locations were repeated, for example 2 and 18. The end points of the probing excursions delineate the yield loci in strain space when only one yield locus probing occurred at that strain, which illustrates the extensive strain hardening which was generated, and this applies also in stress space because the elastic constants are not changed by plastic flow.

Figures 6a and 6b give details of the yield surfaces measurements for stations 6 and 14, respectively. The broken lines indicate the direction of the strain-rate vector ($\dot{\varepsilon}$, $\dot{\gamma} / \sqrt{3}$) along the side of the polygon traversed just before the probing. The stress points shown are automatically plotted from the computer output. From the probing measurements it is generally observed that the yield locus exhibits a protruding rounded nose in the direction of the strain-rate vector with a flattened rear which involves appreciable scatter. Why the latter occurs is clarified in Figure 7. When the probing is in the general direction of the immediately preceding plastic strain-rate vector, the onset of plasticity is closer to that for intermittent loading in a tension test, whereas for the flattened rear of the yield surface the situation is closer to tension followed by compression. For a given strain offset the $\Delta\sigma$ is larger and more variable in the case of reversed straining because of the larger and more rapidly changing tangent modulus.

Examination of the yield loci established that the measured points on the rounded noses closely approximate a circular geometry. To check this analytically, least-squares fits of circles through 6, 8 and 12 measured points on the nose were evaluated. Examples of such circles are shown in Figures 6a and 6b and indicate a good representation of the measured points. Such circular yield loci constitute combined isotropic-kinematic hardening, the radius of the circle expressing the isotropic component and the coordinates of the center, (σ_α , $\sqrt{3}\,\tau_\alpha$), the back-stress vector in tension-torsion space, expressing the anisotropic component of the hardening. In general straining the yield locus is a circle in stress deviator

space with center the back stress tensor α.

Many technological metal forming problems are governed by plastic deformation occurring on the nose of the associated yield surface because the objective of forming is to change the shape of a workpiece to produce a prescribed product so that the process is continuously generating similar changes of geometry. Thus the strain-rate tensor is oriented in a restricted sector of strain-rate space which forms the rounded nose of the yield locus. In this circumstance, analytical investigation of the development of metal-forming defects which may be generated during forming, can be carried out on the basis of combined isotropic-kinematic hardening. This is convenient both from the standpoint of measuring the needed physical characteristics and also of applying the associated theory.

Figure 8 shows the evolution of the back-stress vector, (σ_α , $\sqrt{3}\,\tau_\alpha$), the centers of least-squares fitted yield loci, based respectively on the 8 and 12 probed yield points on the rounded noses of the yield loci. The plotted points correspond to the stations shown in Figure 5, so that the initial tensile straining and traverse of the regular-polygonal path are indicated. The initial yield locus at station 1 shows that the material supplied already exhibited a slightly anisotropic yielding behavior. The shear strain magnitudes were of the order 2% corresponding to a maximum material line rotation of about 1°, whereas the back stress α rotated through about 330°. Thus the rotation of the anisotropic yield loci characteristics completely overwhelms the material rotation.

3. The Structure of the Constitutive Relation

The general theory of elastic-plastic deformation at finite strain, with the strain-hardening-induced anisotropy modeled as combined isotropic-kinematic hardening, was presented in Agah-Tehrani et al. (J. Mech. Phys. of Solids, Vol.35, pp.519-539, 1987). As explained there, for general plasticity analysis it is appropriate to adopt the Kirchhoff stress $\bar{\tau}$ ($\det V^e$ times the Cauchy or true stress) where V^e is the symmetric elastic deformation gradient. Since in almost all problems, other than high-pressure shock-wave analysis, $\det V^e$,

the volume ratio of the elastically deformed material to the unstressed material is almost unity, $\boldsymbol{\tau}$ is effectively equal to the true-stress tensor $\boldsymbol{\sigma}$.

The change in the yield surface due directly to *plastic flow* is termed strain hardening. It is part of a flow or incremental type process in that the rate of change of the yield surface relative to axes fixed in space is determined by the rate of plastic straining plus a contribution arising from the spin of the yield surface because it is embedded in the deforming material. For isotropic-kinematic hardening, the back stress α embodies the anisotropic part of the changing yield condition which shifts the center of the yield surface away from the origin in stress space. The size of the yield surface expresses the isotropic component of the hardening. Thus the evolution equation governing the anisotropic component of the hardening due to plastic flow must involve the variable $\dot{\alpha}$, the total rate change of α, less the contribution of the material spin W, giving the appropriate yield-surface variable:

$$\dot{\alpha} - (W\alpha - \alpha W) = \dot{\alpha} - W\alpha + \alpha W = \alpha \tag{3.1}$$

which is the Jaumann derivative. The term $(W\alpha - \alpha W)$ expresses the rate of change of a spinning constant tensor (Lee et al., J. Appl. Mech., Vol.50, pp.554-560, 1983).

Plasticity comprises the stress-motivated flow of dislocations and other mechanisms through a crystal lattice which produces permanent deformation. Strain hardening expresses the impediment to such migration built up by previous plastic flow which disturbs the initial level of uniformity of the crystal lattice. The anisotropy of the hardening arises because pile-ups of dislocations against barriers in the crystal structure impede flow more strongly in the direction of the flow which produced them. Thus the evolution equation for the back stress α expresses its rate of growth in terms of the plastic strain rate D^p and the current value of α itself. D^p is the macroscopic quantity which incorporates the amplitude of the flow and its direction while α expresses the strength and orientation of the resistance to continued plastic flow. Since the Jaumann rate of α, the appropriate variable for the rate of change of α, is a symmetric second order tensor, it must be representable by an isotropic, symmetric tensor function of α and D^p. Thus the general form which the evolution equation for α must take

is:

$$\alpha = h(\alpha, D^p) = \eta_1 D^p + \eta_2 \bar{D}^p \alpha + \eta_3 \bar{D}^p (\alpha^2 - (\mathrm{tr}\alpha^2) I/3)$$
$$+ \eta_4 (\alpha D^p + D^p \alpha - 2\mathrm{tr}(\alpha D^p) I/3)$$
$$+ \eta_5 (\alpha^2 D^p + D^p \alpha^2 - 2\mathrm{tr}(\alpha^2 D^p/3) I) \qquad (3.2)$$

where $\bar{D}^p = (2\mathrm{tr}(D^p D^p)/3)^{1/2}$ is the generalized scalar plastic strain rate and the η's are functions of the invariants of α. It is linear in D^p to preserve the rate independent plastic response under consideration. Special cases are commonly utilized in which some of the η's are taken to be zero. If η_1 is the only nonzero coefficient, (3.2) reduces to the rule first suggested by Prager when he introduced the concept of kinematic hardening.

4. Determination of the Constitutive Relation

The plan of our research program is to carry out experiments in which tubes are deformed in tension-torsion space, involving a series of prescribed straining paths, and to record the resulting stress and yield loci histories in order to determine the structure of the evolution equation for the back stress. Usually only one of the terms have been included in applications of (3.2). In view of the detailed information concerning the growth of the back stress achieved on the current project, the inclusion of three terms in the evolution equation is investigated. For the tension-torsion of a thin walled tube, the evolution equations for the back stresses (3.2) can then be reduced to

$$\dot{\alpha}_1 = \eta_1 D_1^p + \eta_2 \bar{D}^p \alpha_1 + \eta_3 \bar{D}^p (\frac{2}{3}\alpha_1^2 - \frac{1}{3}\alpha_2^2 - \frac{1}{3}\alpha_3^2 + \frac{1}{3}\alpha_{12}^2) + 2\alpha_{12} D_{12} \qquad (4.1)$$

$$\dot{\alpha}_2 = \eta_1 D_2^p + \eta_2 \bar{D}^p \alpha_2 + \eta_3 \bar{D}^p (-\frac{1}{3}\alpha_1^2 + \frac{2}{3}\alpha_2^2 - \frac{1}{3}\alpha_3^2 + \frac{1}{3}\alpha_{12}^2) - 2\alpha_{12} D_{12} \qquad (4.2)$$

$$\dot{\alpha}_{12} = \eta_1 D_{12}^p + \eta_2 \bar{D}^p \alpha_{12} + \eta_3 \bar{D}^p (\alpha_1 + \alpha_2)\alpha_{12} + (\alpha_2 - \alpha_1) D_{12} \qquad (4.3)$$

when η_4 and η_5 are set to zero. Here subscripts 1, 2, 3 and 12 represent the axial, circumferential, radial and shear components of α, $\dot{\alpha}$, D^p and D and D is the rate of

deformation tensor. The experimental record consists of information on the true stresses $\bar{\sigma}_1$, $\bar{\sigma}_{12}$ and the logarithmic strains ε_1, ε_2 and ε_{12}. From these data, the accumulated plastic strains and the accumulated generalized plastic strain histories can be evaluated. In the $(\bar{\sigma}_1, \sqrt{3}\bar{\sigma}_{12})$ stress space the center of a circular yield surface corresponds to the back stress components $(3/2)\alpha_1$ and $\sqrt{3}\alpha_{12}$. Thus, we may curve-fit a circular geometry through the rounded-nose portion of the experimentally determined yield surface and obtain α_1 and α_{12} from the center of the circle. All of these results allow us to tabulate ε_1^p, ε_2^p, ε_{12}^p, ε_{12}, α_1 and α_{12} against $\bar{\varepsilon}^p$ at the yield surface probing stations. Here we have employed the definitions $\varepsilon^p \equiv \int D^p(t)dt$, $\varepsilon \equiv \int D(t)dt$ and $\bar{\varepsilon}^p \equiv \int \bar{D}^p(t)dt$. These are introduced as convenient mathematical variables in terms of which to express this incremental or rate type theory in which the velocity gradient, D, is the strain rate type variable used. They are not finite strain components because the material rotates and the strain increments apply to varying material directions in the body. We next smooth these tabulated results by fitting polynomials through these data to obtain continuous representations of these quantities as functions of $\bar{\varepsilon}^p$. To extract the η's we may recast (4.1) to (4.3) as

$$\frac{d\alpha_1}{d\bar{\varepsilon}^p} = \eta_1 \frac{d\varepsilon_1^p}{d\bar{\varepsilon}^p} + \eta_2\alpha_1 + \eta_3\left(\frac{2}{3}\alpha_1^2 - \frac{1}{3}\alpha_2^2 - \frac{1}{3}\alpha_3^2 + \frac{1}{3}\alpha_{12}^2\right) + 2\alpha_{12}\frac{d\varepsilon_{12}}{d\bar{\varepsilon}^p} \tag{4.4}$$

$$\frac{d\alpha_2}{d\bar{\varepsilon}^p} = \eta_1 \frac{d\varepsilon_2^p}{d\bar{\varepsilon}^p} + \eta_2\alpha_2 + \eta_3\left(-\frac{1}{3}\alpha_1^2 + \frac{2}{3}\alpha_2^2 - \frac{1}{3}\alpha_3^2 + \frac{1}{3}\alpha_{12}^2\right) - 2\alpha_{12}\frac{d\varepsilon_{12}}{d\bar{\varepsilon}^p} \tag{4.5}$$

$$\frac{d\alpha_{12}}{d\bar{\varepsilon}^p} = \eta_1 \frac{d\varepsilon_{12}^p}{d\bar{\varepsilon}^p} + \eta_2\alpha_{12} + \eta_3(\alpha_1 + \alpha_2)\alpha_{12} + (\alpha_2 - \alpha_1)\frac{d\varepsilon_{12}}{d\bar{\varepsilon}^p} \tag{4.6}$$

Since α is a deviator, α_3 can be expressed as

$$\alpha_3 = -(\alpha_1 + \alpha_2) \tag{4.7}$$

All the quantities in these three evolution equations, except the η's, α_2 and $(d\alpha_2)/(d\bar{\varepsilon}^p)$, are now available. Since α_2 cannot be determined, and hence $(d\alpha_2)/(d\bar{\varepsilon}^p)$, from direct experimental measurements, we employ normality cast in the form:

$$\frac{(d\varepsilon_1^p)/(d\bar{\varepsilon}^p)}{(2/3)\,\bar{\sigma}_1 - \alpha_1} = \frac{(d\varepsilon_{12}^p)/(d\bar{\varepsilon}^p)}{\bar{\sigma}_{12} - \alpha_{12}} = \frac{(d\varepsilon_2^p)/(d\bar{\varepsilon}^p)}{-(1/3)\,\bar{\sigma}_1 - \alpha_2} \tag{4.8}$$

to express α_2 alternatively as:

$$\alpha_2 = -\frac{1}{3}\bar{\sigma}_1 - \frac{d\varepsilon_2^p}{d\varepsilon_1^p}\left(\frac{2}{3}\bar{\sigma}_1 - \alpha_1\right) \tag{4.9}$$

or

$$\alpha_2 = -\frac{1}{3}\bar{\sigma}_1 - \frac{d\varepsilon_2^p}{d\varepsilon_{12}^p}\left(\bar{\sigma}_{12} - \alpha_{12}\right) \tag{4.10}$$

This allows us to infer an averaged value of α_2 as a function of $\bar{\varepsilon}^p$ from these two expressions. To gain confidence in this approximate procedure, we estimate the conformance of the associated flow rule from the first equality of (4.8). If the associated flow rule can be established to within experimental scatter, we perform polynomial fitting on the averaged α_2 and determine its slope, $(d\alpha_2)/(d\bar{\varepsilon}^p)$, from such a continuous representation. With this last piece of information determined, we can estimate the η's as functions of $\bar{\varepsilon}^p$ from (4.4) to (4.6). Since we also can obtain the invariants of α as functions of $\bar{\varepsilon}^p$, we can eliminate $\bar{\varepsilon}^p$ in order to extract the structure of the η's in terms of the invariants of α.

The polygonal straining path employed in the experiments described above involves corners. As the straining direction is changed from one side to the next as a corner is traversed, the direction of the stress rate vector lags behind that of the strain rate vector due to the influence of elasticity. Normality is established only after the stress rate vector catches up with the strain rate vector. For the case of the polygonal straining path, the strain path length of each straight segment is not long enough for this to occur. However, as explained above, normality has to be relied upon in order to infer approximately the circumferential back stress α_2 due to the unavailability of appropriate experimental measurement. Thus the measurement from the polygonal straining path is not ideal for determining the structure of the η's. As a result of this, we selected another set of straining paths which were designed to minimize

such corner effects. The four straining paths in the axial-generalized-shear strain space, consisting of two proportional straining paths and two slightly nonproportional straining paths, are shown in Figure 9a-d. The specimens were prepared from Al-Mn and the specimen designation associated with each straining path is also indicated. The corresponding stress responses from these four tests in the axial-generalized-shear stress space are shown in Figures 10a-d. The measurements from these tests were reduced to a form suitable for the extraction of the η's as described above. Some typical polynominal fits of the data are shown in Figures 11a-b. These are for the stresses, $\bar{\sigma}_1$ and $\bar{\sigma}_{12}$, of the proportional path 34g2. Figure 12 shows the trajectories of the centers of the fitted circular yield loci in the axial-generalized-shear stress space.

For each straining history, we can solve for the values of η_1, η_2, and η_3 from (4.4) to (4.6) at each level of $\bar{\varepsilon}^p$, using the continuous representations of the variables obtained from the experimental data. The values of η's as a function of the invariant $\bar{\alpha}$, defined as $\bar{\alpha} \equiv (\mathrm{tr}\alpha^2)^{1/2}$, for these paths are inconsistent. Attempts to extract η_1 and η_2 from the experimental data by setting η_3 in the evolution equation to zero also did not yield consistent results. We therefore solved for η_1 from the experimental data by setting both η_2 and η_3 in the evolution equation to zero. The values of η_1 were obtained from the reduced form of (4.4) to (4.6) for each level of $\bar{\varepsilon}^p$ using the least-squares method. Figure 13 shows the plot of η_1 versus $\bar{\alpha}$ for the four straining paths. The four curves do not collapse into one. However, the two proportional straining paths, 34g2 and 34g3, do show a certain degree of correspondence. Thus we curve-fitted the values of η_1 from these two sets of proportional straining data to obtain the relation

$$\eta_1(\bar{\alpha}) = m_0 + m_1 \bar{\alpha} + m_2 \bar{\alpha}^2$$

where $m_0 = 1104.2\mathrm{MPa}$, $m_1 = -11.3$ and $m_3 = -0.15\mathrm{MPa}^{-1}$. Using such a function representation for η_1, we went back to the data from the nonproportional straining paths 34g1 and 34f3 and solved for η_2 and η_3 from (4.4) - (4.6) using the least-squares method. The resulting η_2 and η_3 obtained from the 34f3-straining-path data are

$$\eta_2(\bar{\alpha}) = n_0 + n_1\,\bar{\alpha} + n_2\,\bar{\alpha}^2$$

$$\eta_3(\bar{\alpha}) = k_0 + k_1\,\bar{\alpha} + k_2\,\bar{\alpha}^2$$

where $n_0 = 76.1\text{MPa}$, $n_1 = -2.4$, $n_2 = -0.0019\text{MPa}^{-1}$, $k_0 = 7.16\text{MPa}$, $k_1 = -0.48$ and $k_2 = 0.0092\text{MPa}^{-1}$. The data from the other nonproportional straining path, 34g1, did not yield a satisfactory result. Inspection of the stress history of straining path 34g1 in Figure 10a shows a sharp bend in the curve immediately following the elastic response. We cannot trace the cause of such an unexpected behavior. Hence the data from this nonproportional straining path might not be reliable.

There are thus two sources of complexity involved in our attempt to extract the structure of the functions η_1, η_2 and η_3. Firstly, the circumferential back stress had to be inferred from normality rather than determined from direct measurements. Secondly, inspection of the recorded stress histories in Figures 10a-d indicates that the response started to become jerky midway through each straining history. In future work, it would be advisable to seek the possibility of obtaining more complete experimental data so that the use of normality can be avoided. It would also be advantageous to reduce the noise level of the stress response in the experiments.

5. Conclusions

The findings of this project have established that, for some ductile aluminum alloys, the very significant anisotropy of the plastic-flow characteristics which develop during plastic straining can be quite accurately expressed by combined-isotropic-kinematic hardening theory. This applies for continuing plastic flow, such as occurs in many metal-forming processes. The continuum mechanics theory of combined-isotropic-kinematic hardening is well developed for stress and deformation analysis, which thus offers the opportunity to include the study of the influence of anisotropic material response in forming analyses.

The adoption of tension/compression-torsion testing measurements provided the opportunity to include nonproportional two-dimensional straining trajectories to provide input for developing appropriate constitutive relations. Since plastic deformation is essentially incompressible, the material tensors which occur, such as the back stress, are deviatoric and so can be adequately investigated using two-dimensional testing. However, in order to deduce the appropriate constitutive theory it is *essential* to carry out such measurements. In the engineering literature it has been common to measure the yield stresses in tension and compression, and if they differ, simply adopt an isotropic-kinematic hardening law determined by these two yield points. The present study brings out the importance of more generally based two-dimensional testing in order to deduce reliable constitutive relations for applications.

STRAIN CONTROLLED TENSION TEST

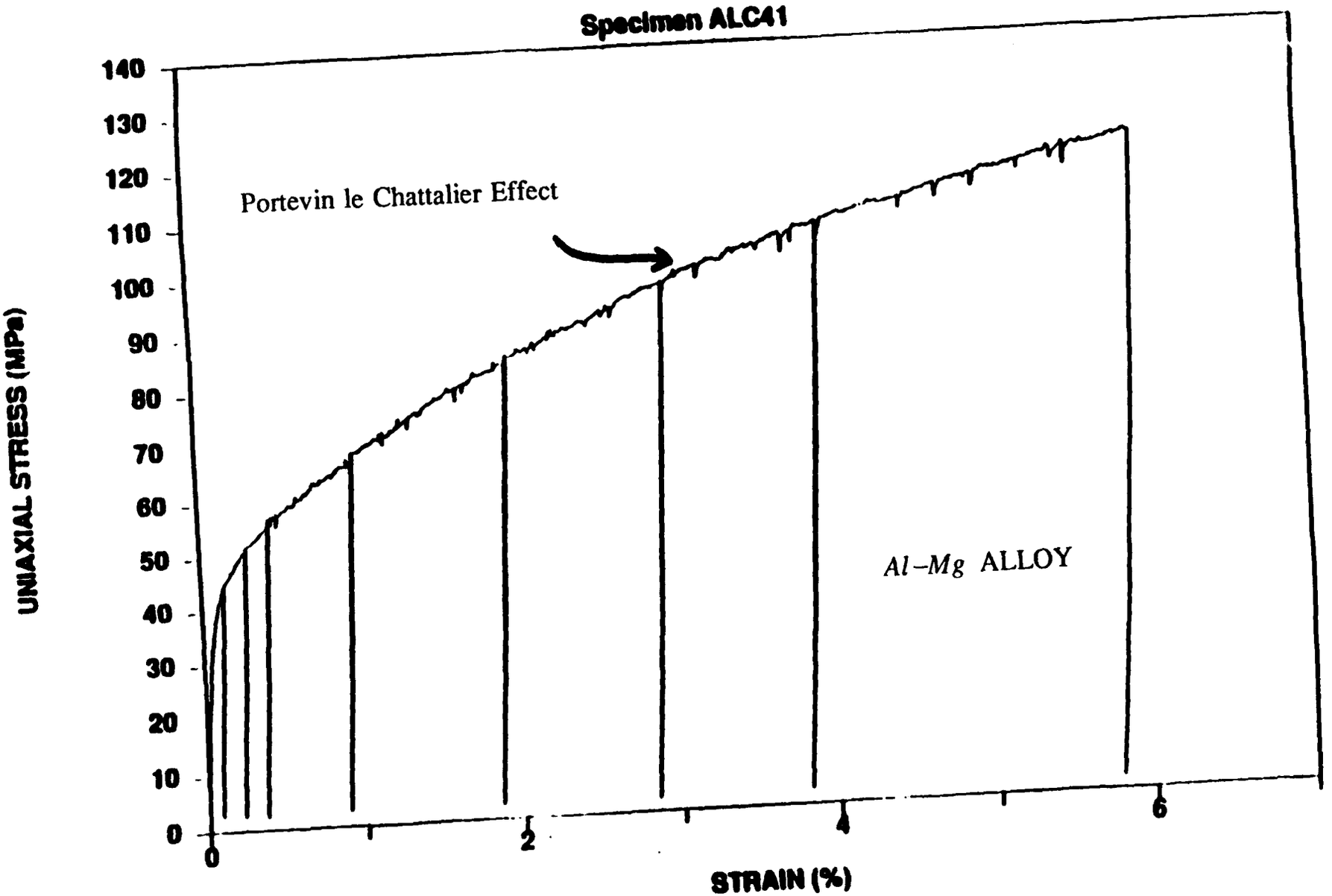

Figure 1 Strain controlled tension test with intermittent unloading and re-loading

STRESS CONTROLLED TENSION TEST

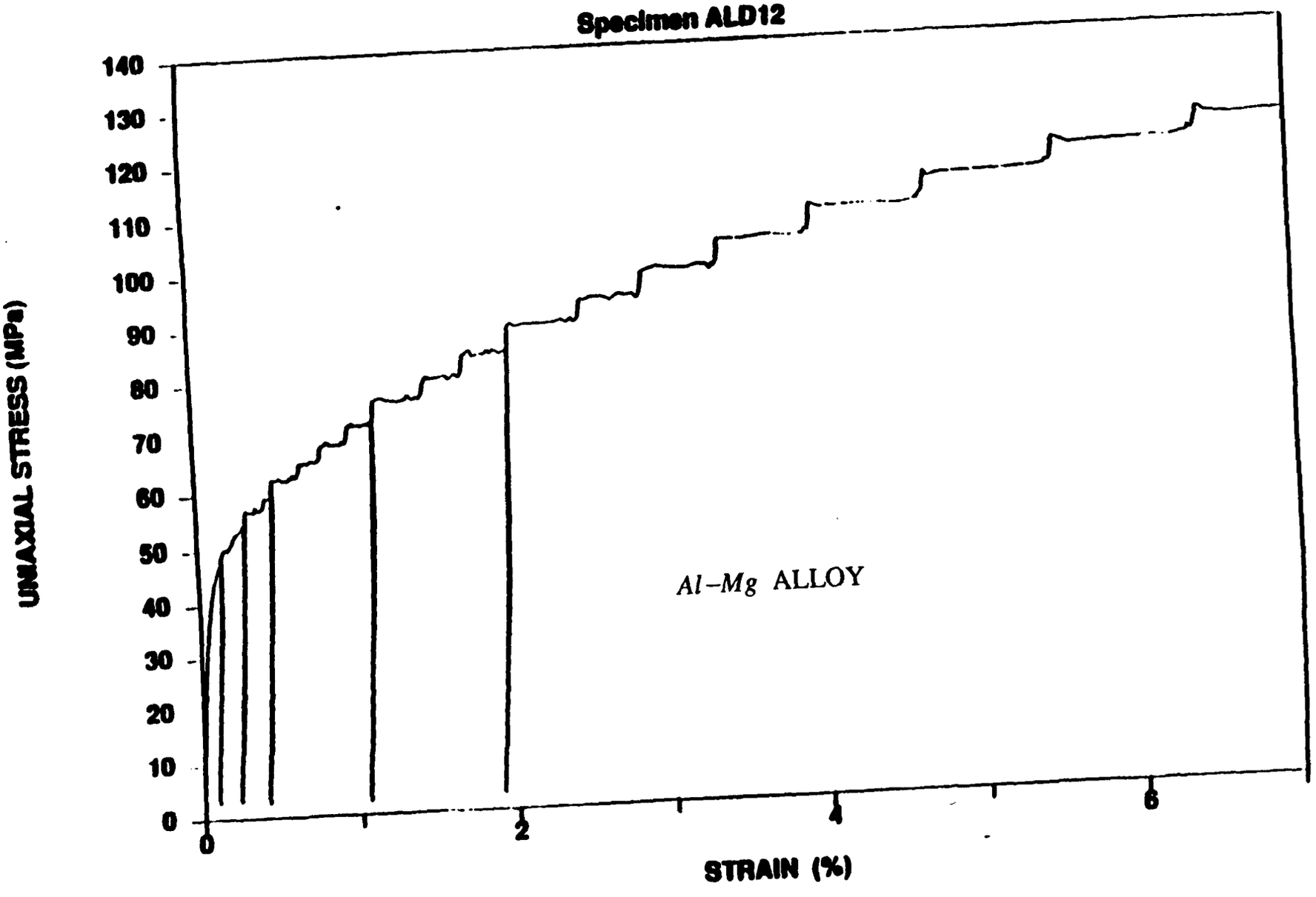

Figure 2 Stress controlled tension test with intermittent unloading and re-loading

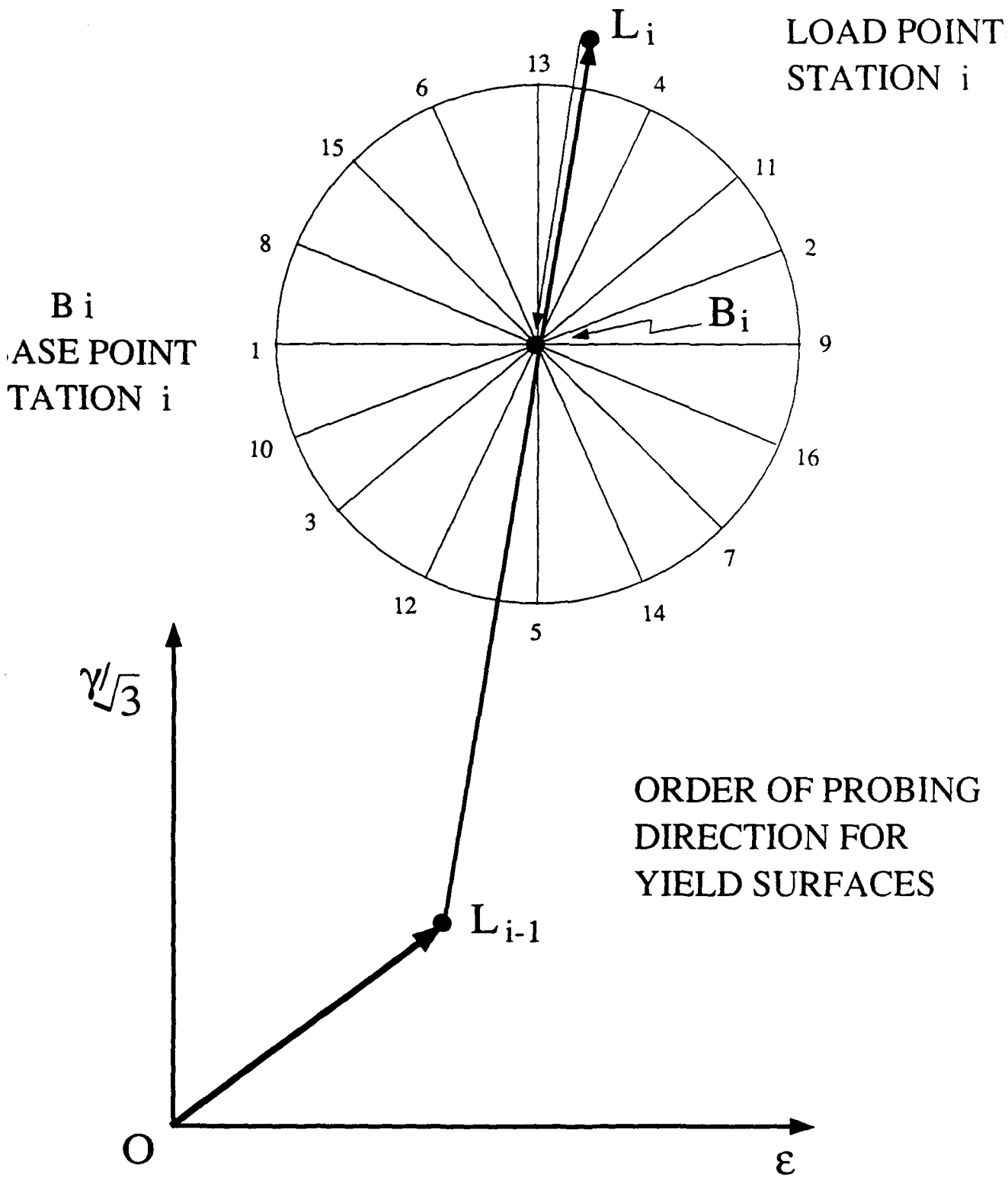

Figure 3 Sequence of 16 excursions used to determine the stresses and strains at the onset of renewed plasticity

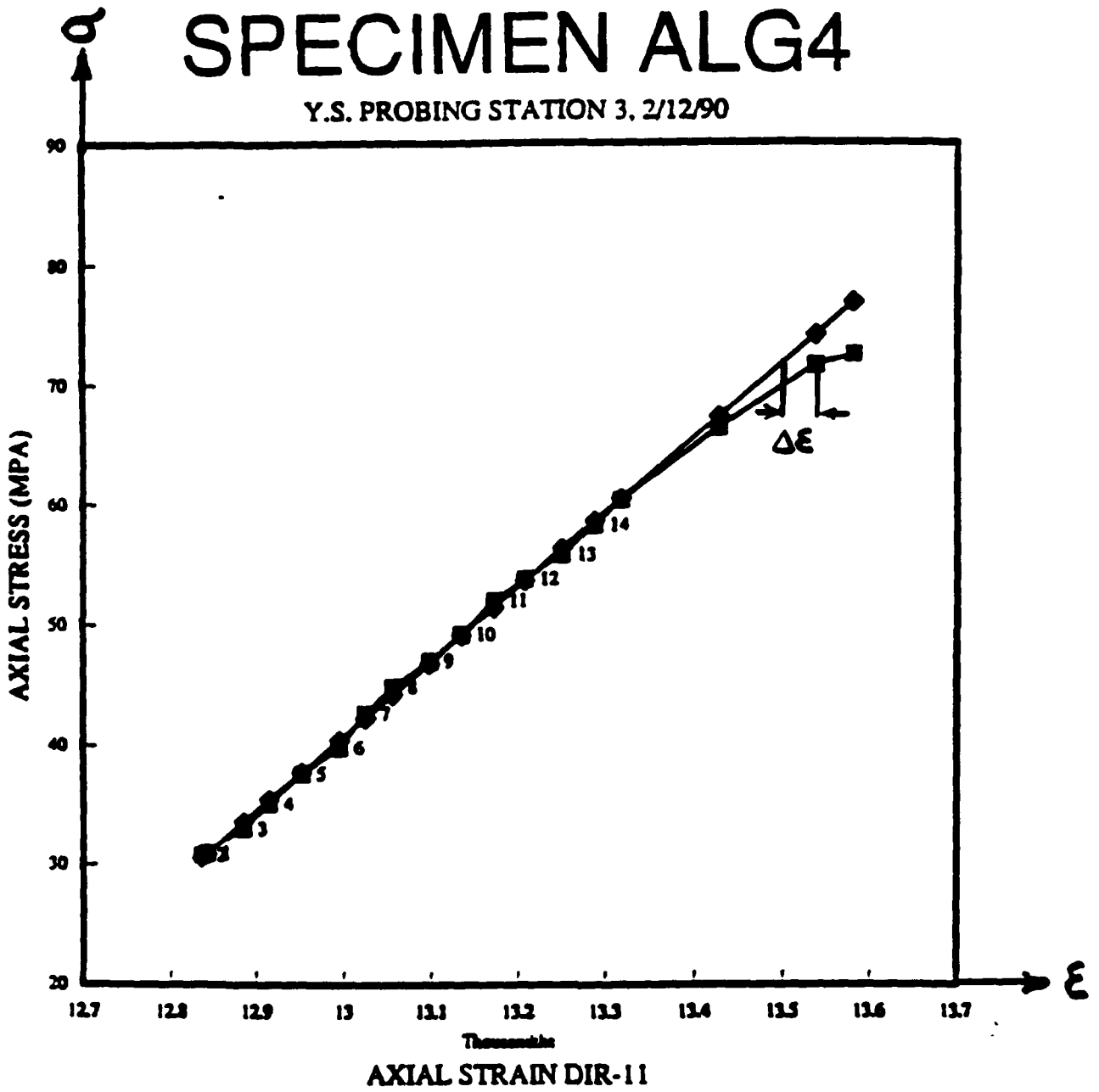

PROBING FROM BASE POINT WITH OFFSET $\sqrt{(\Delta\varepsilon)^2 + (\Delta\gamma/\sqrt{3})^2} \geq 10^{-4}$

Figure 4 An example of the yield locus probing procedure

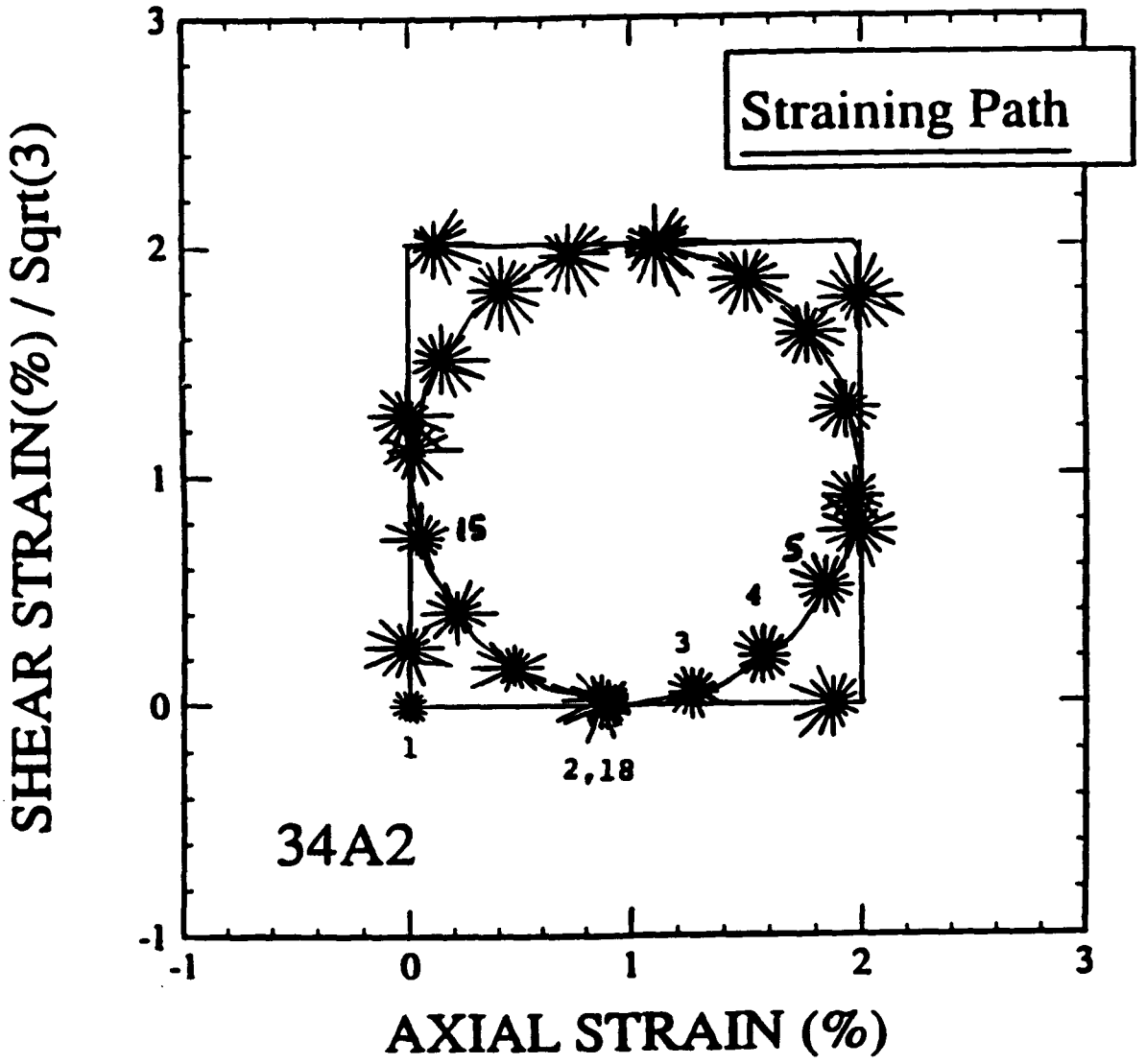

Figure 5 The prescribed strain history of the polygonal and square paths

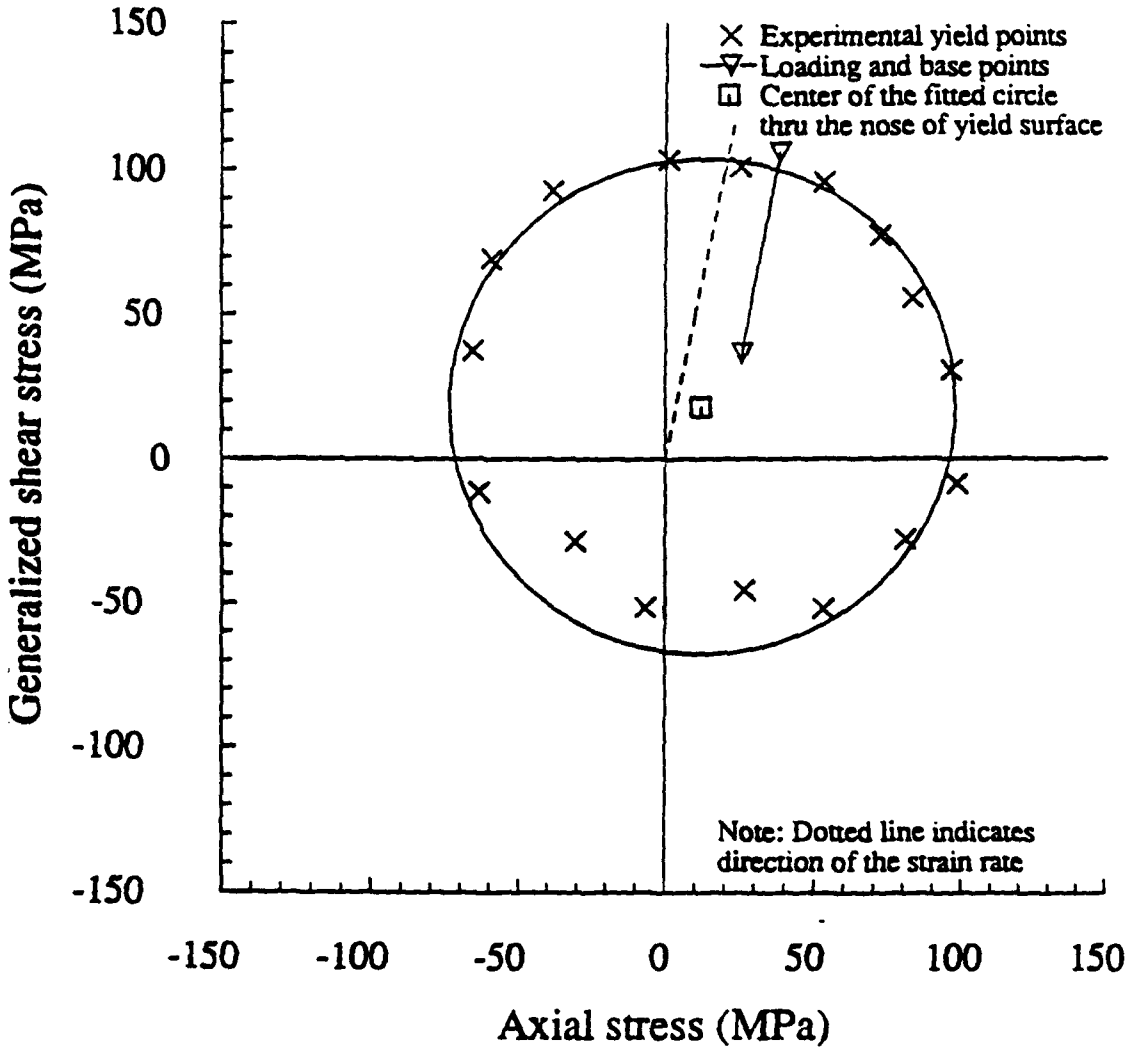

Figure 6a Yield surface measurement for station 6. The center of the fitted circle is related to the back stress α.

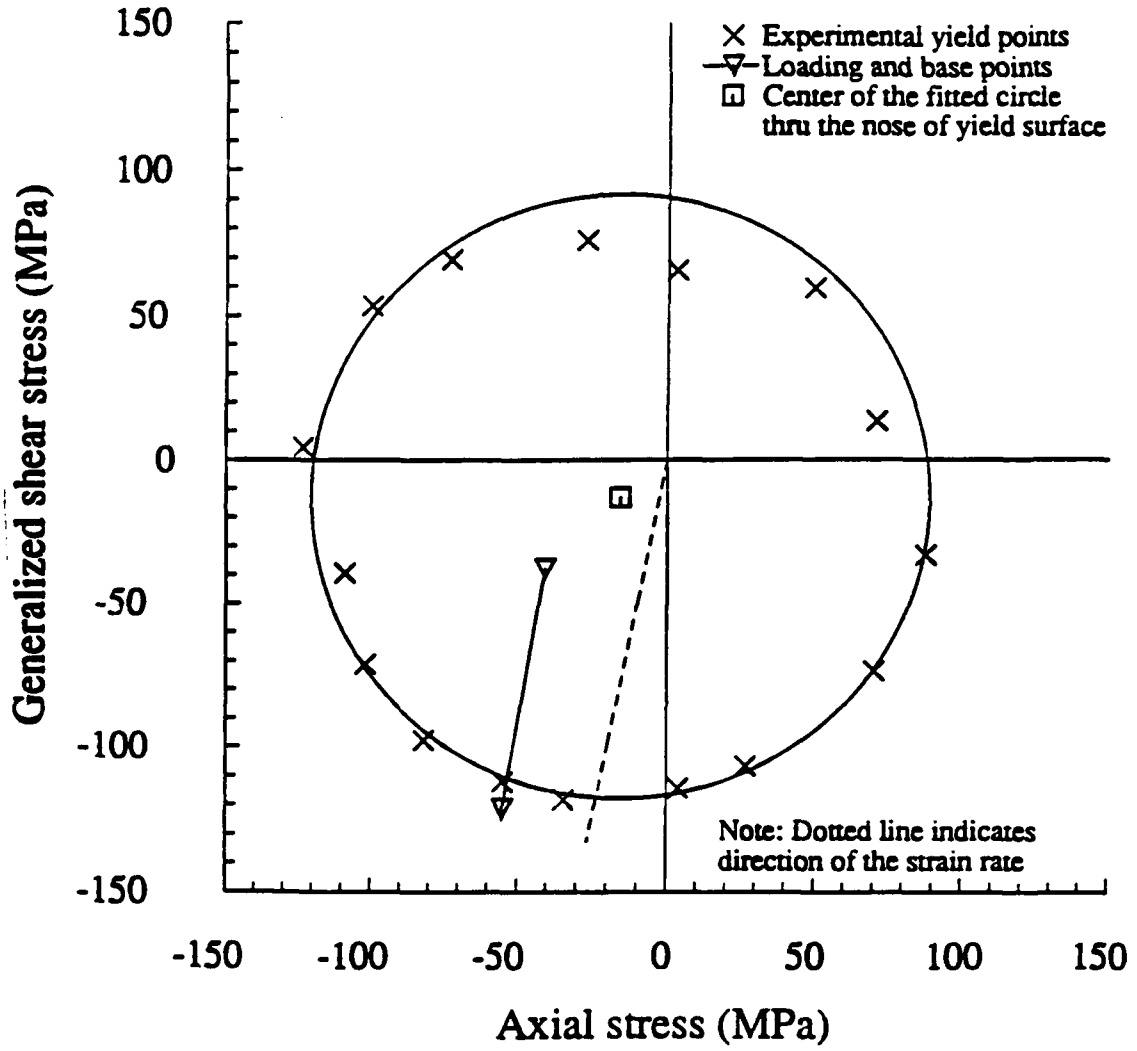

Figure 6b Yield surface measurement for station 14. The center of the fitted circle is related to the back stress α.

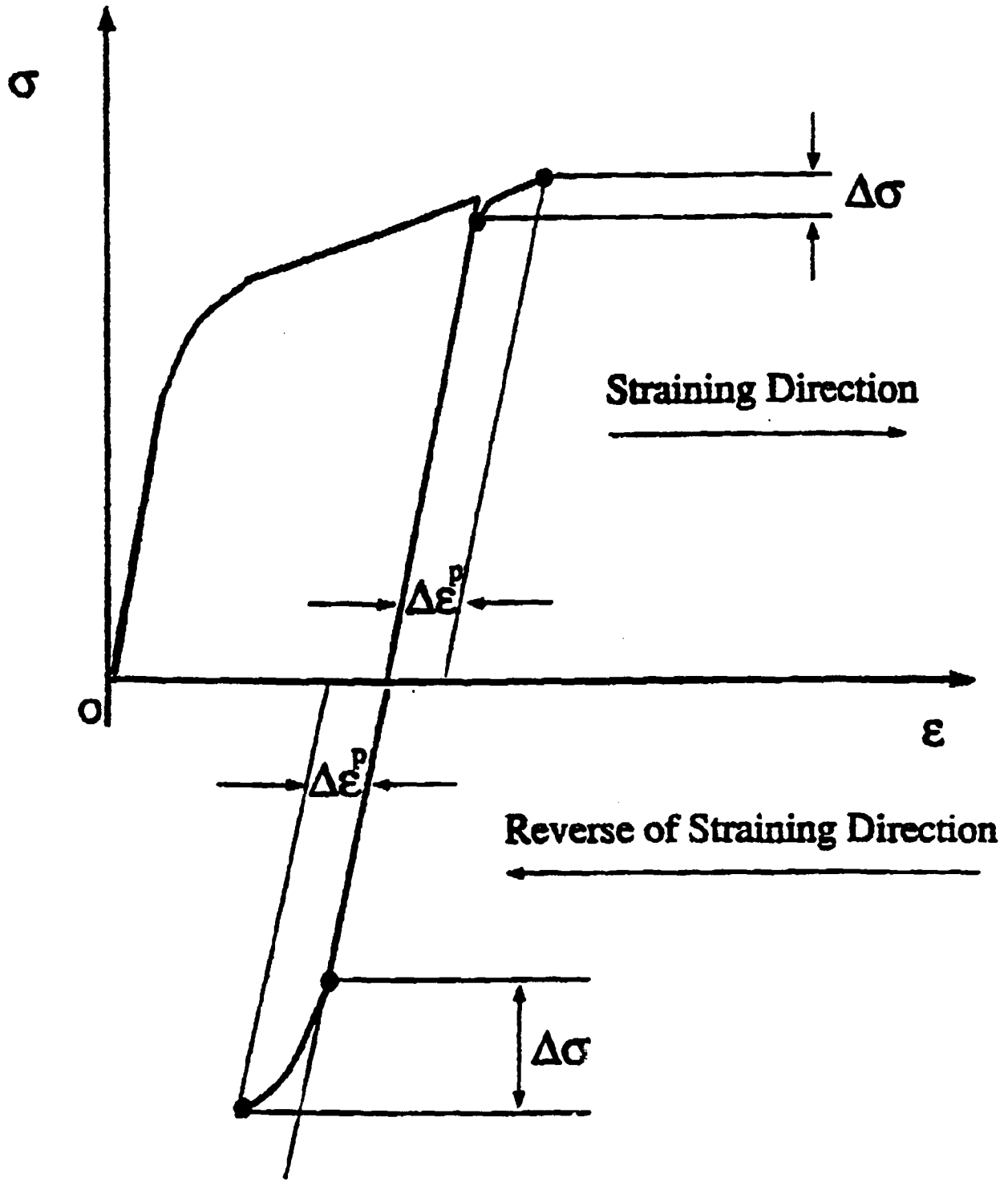

Figure 7 Strain generated by unloading from a tension test followed by re-loading in tension or compression

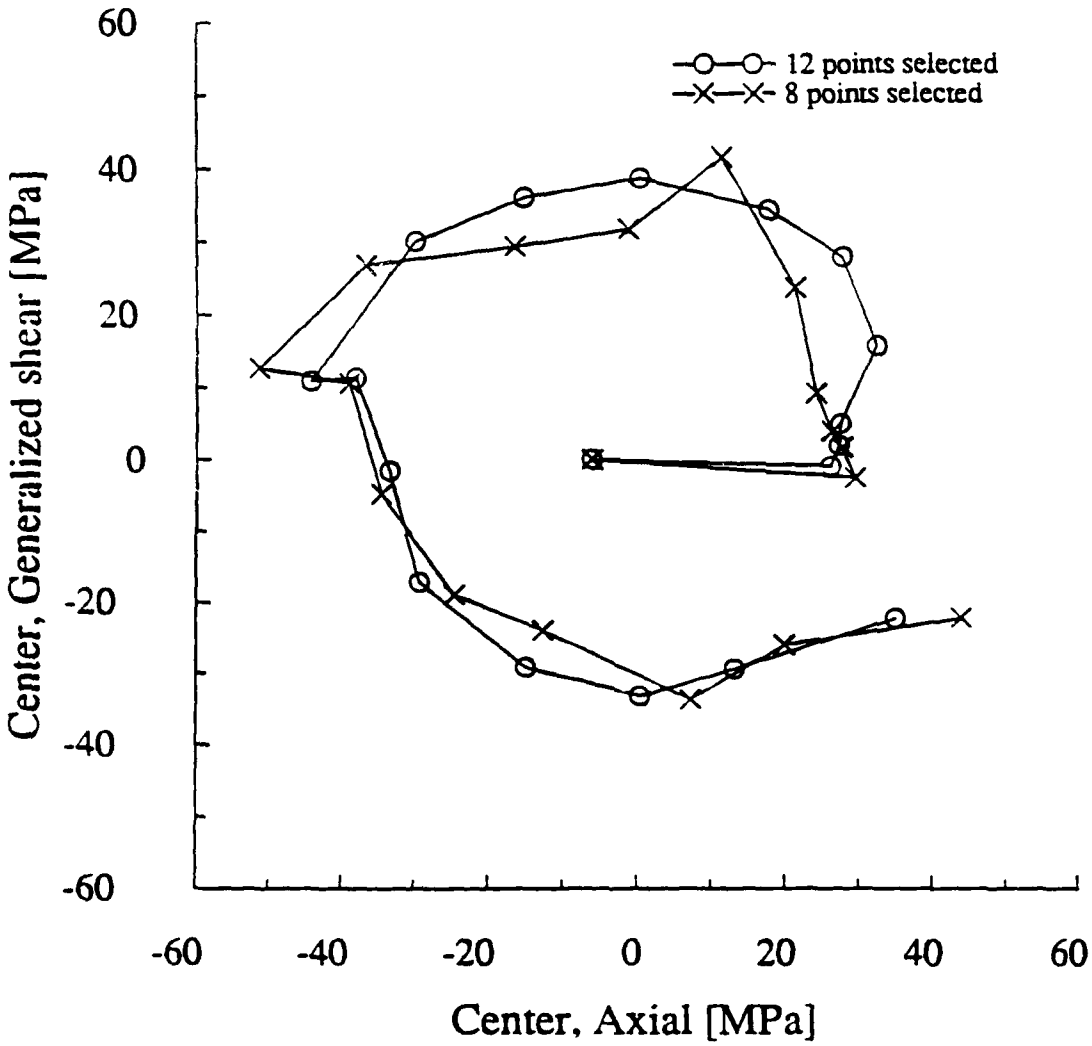

Figure 8 Evolution of the backstress α for the polygonal path

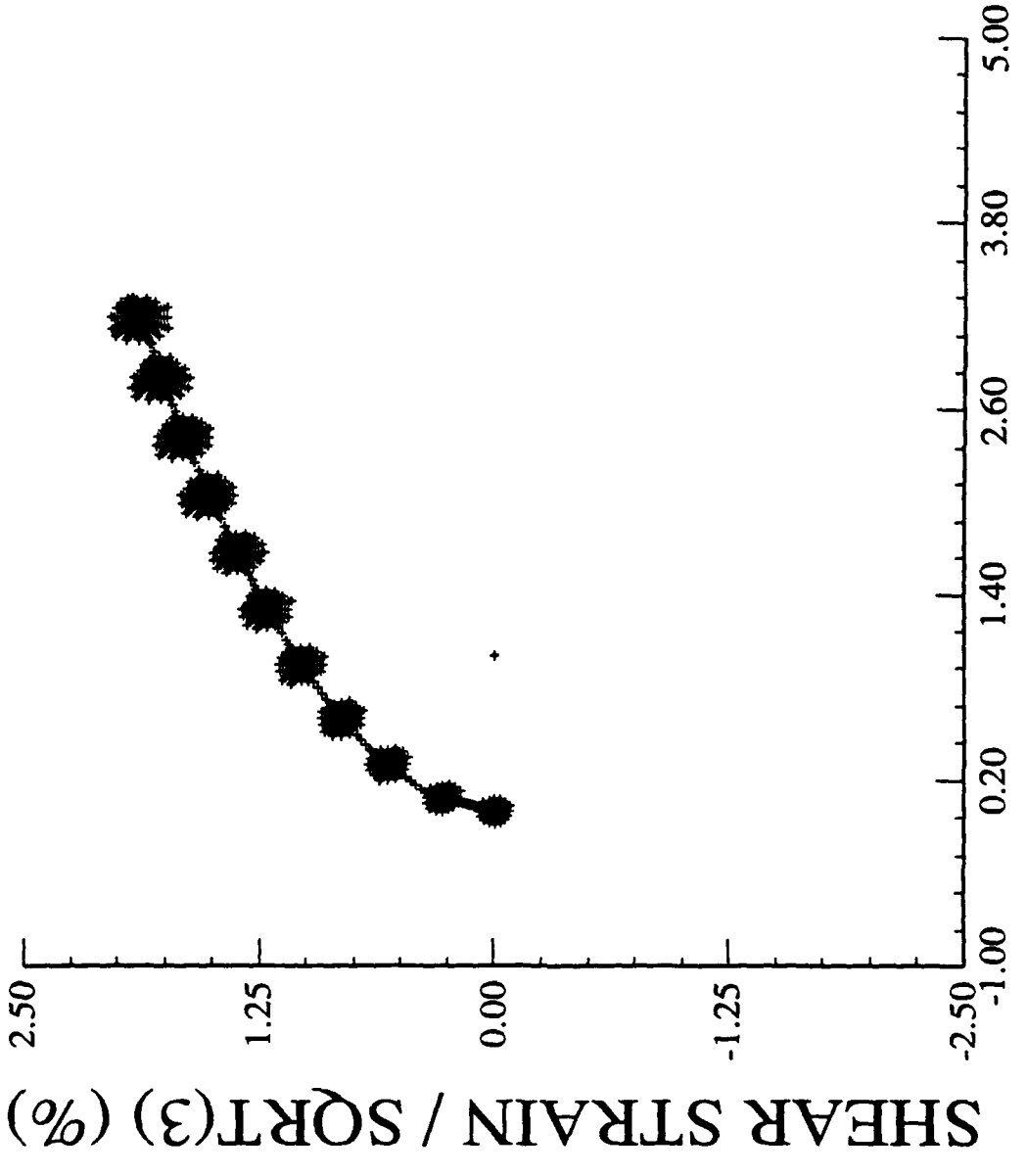

Figure 9a Prescribed nonproportional straining path 34g1

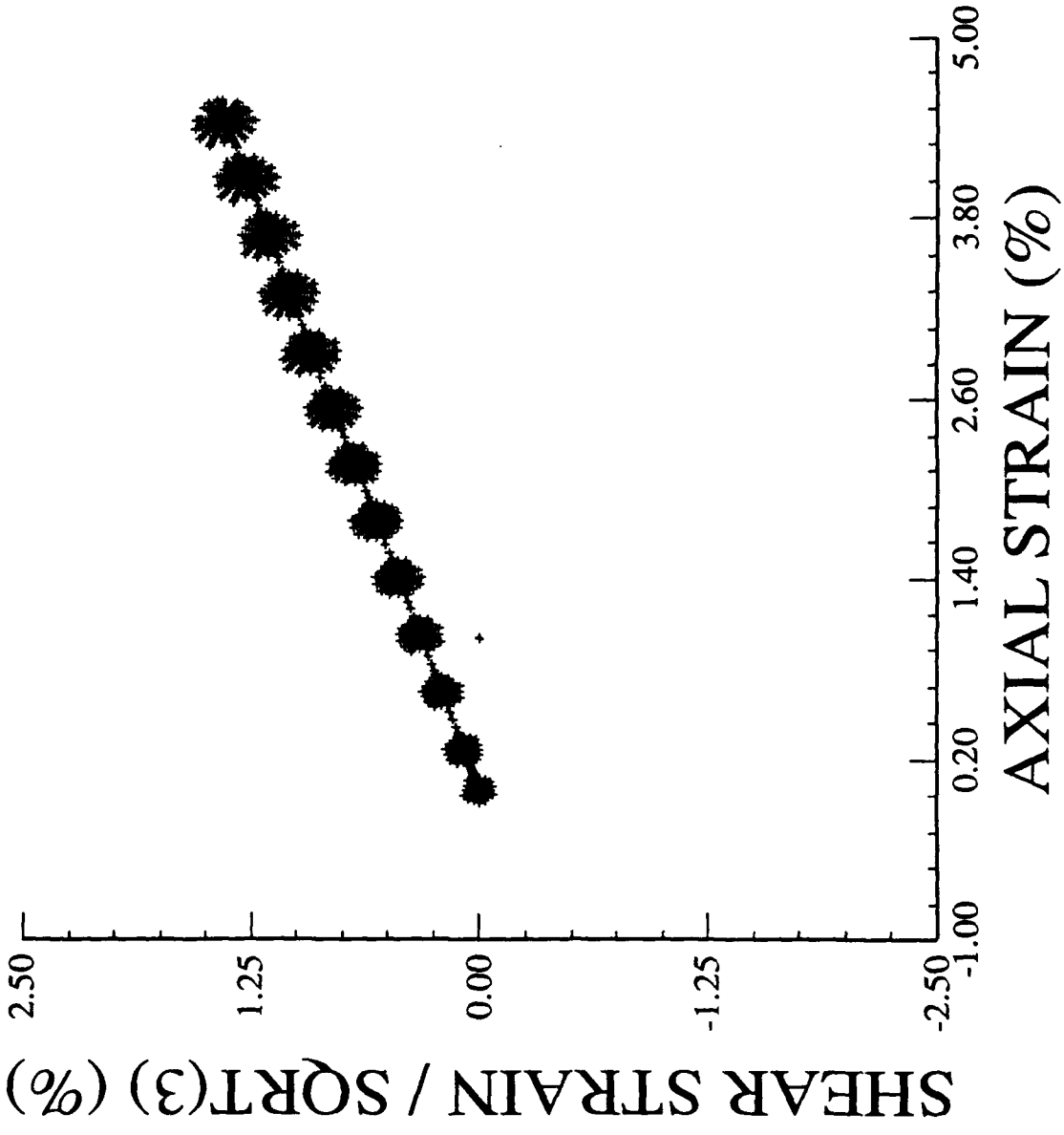

Figure 9b Prescribed proportional straining path 34g2

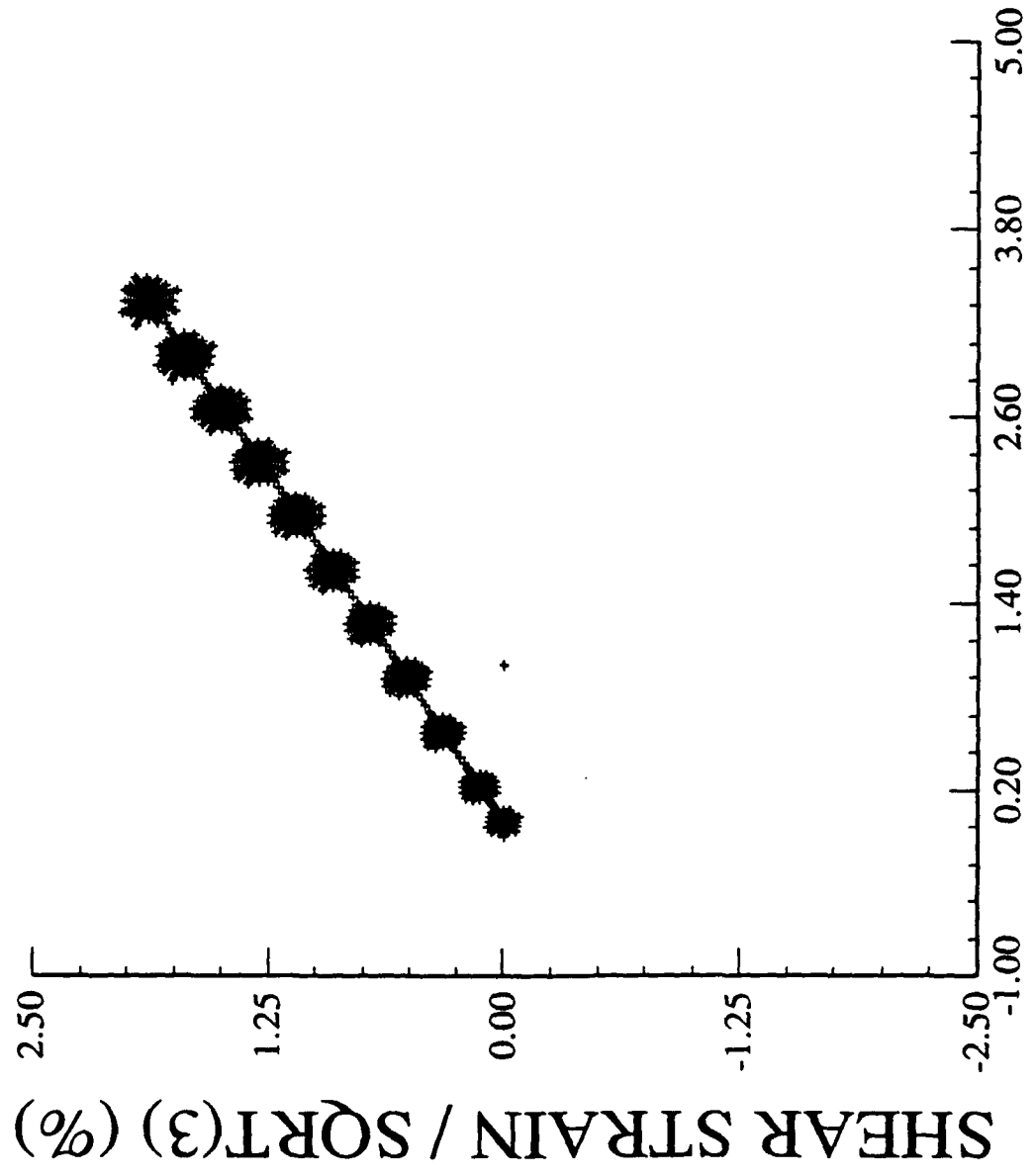

Figure 9c Prescribed proportional straining path 34g3

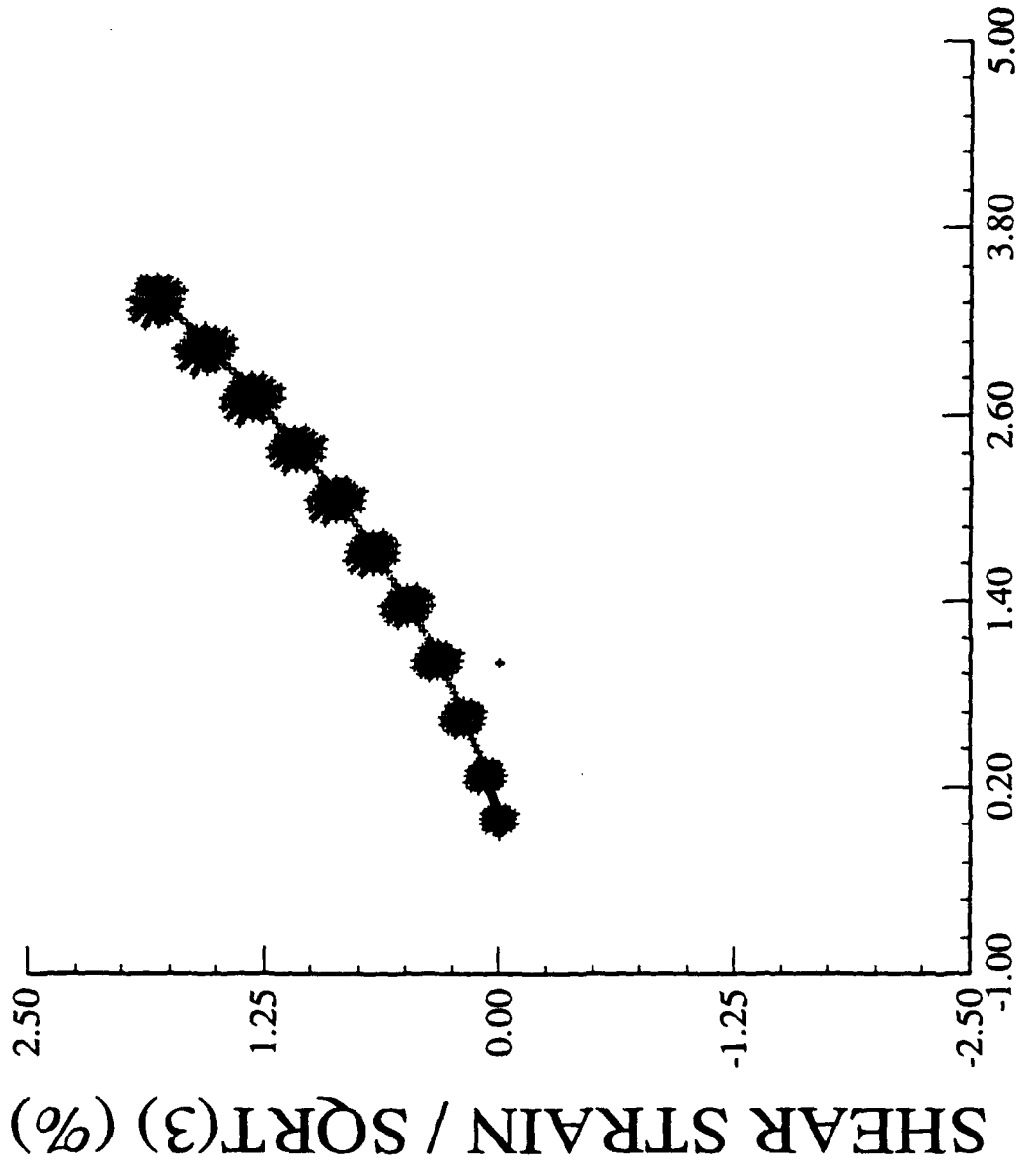

Figure 9d Prescribed nonproportional straining path 34f3

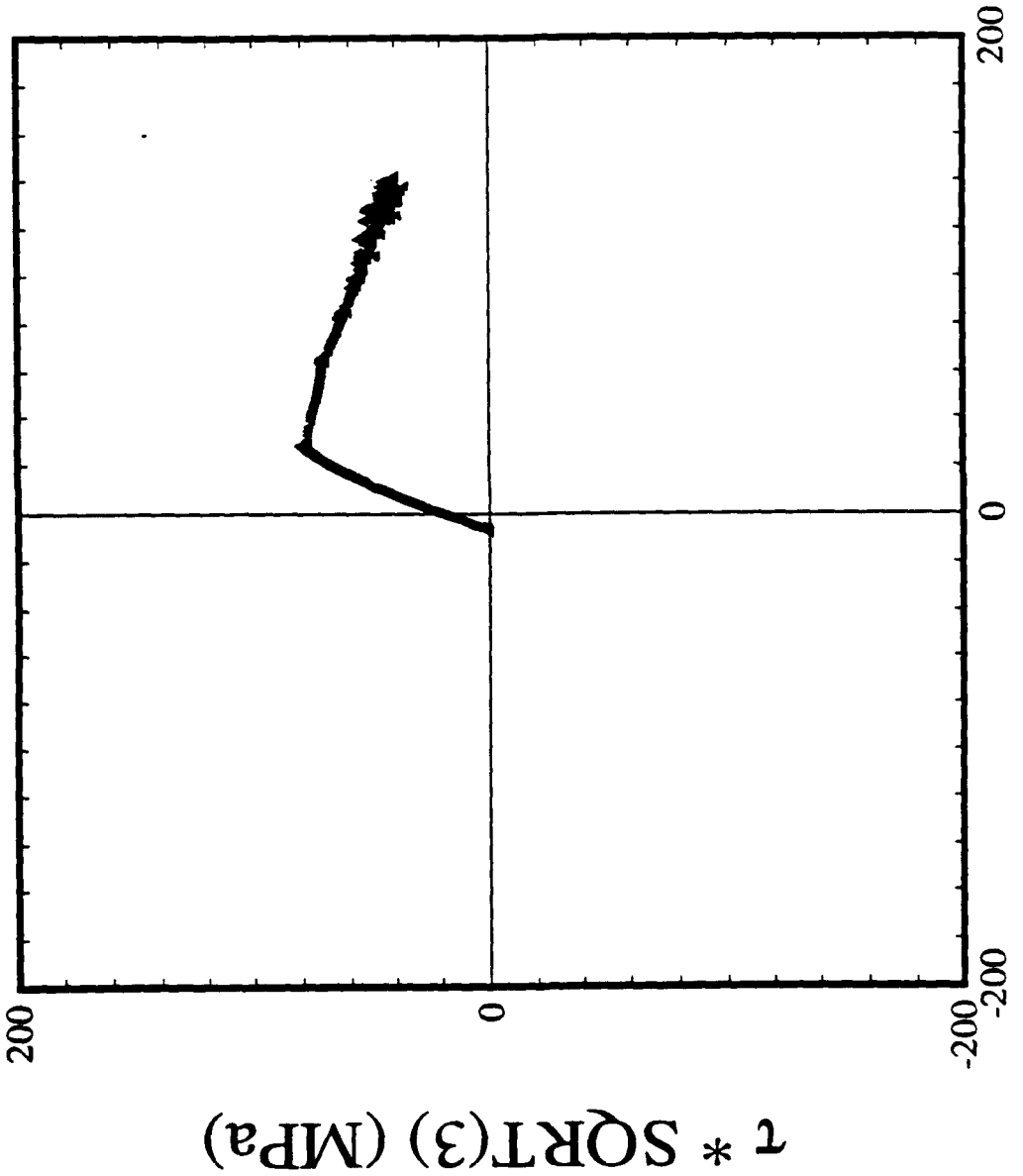

Figure 10a Recorded stress response from nonproportional straining path 34g1

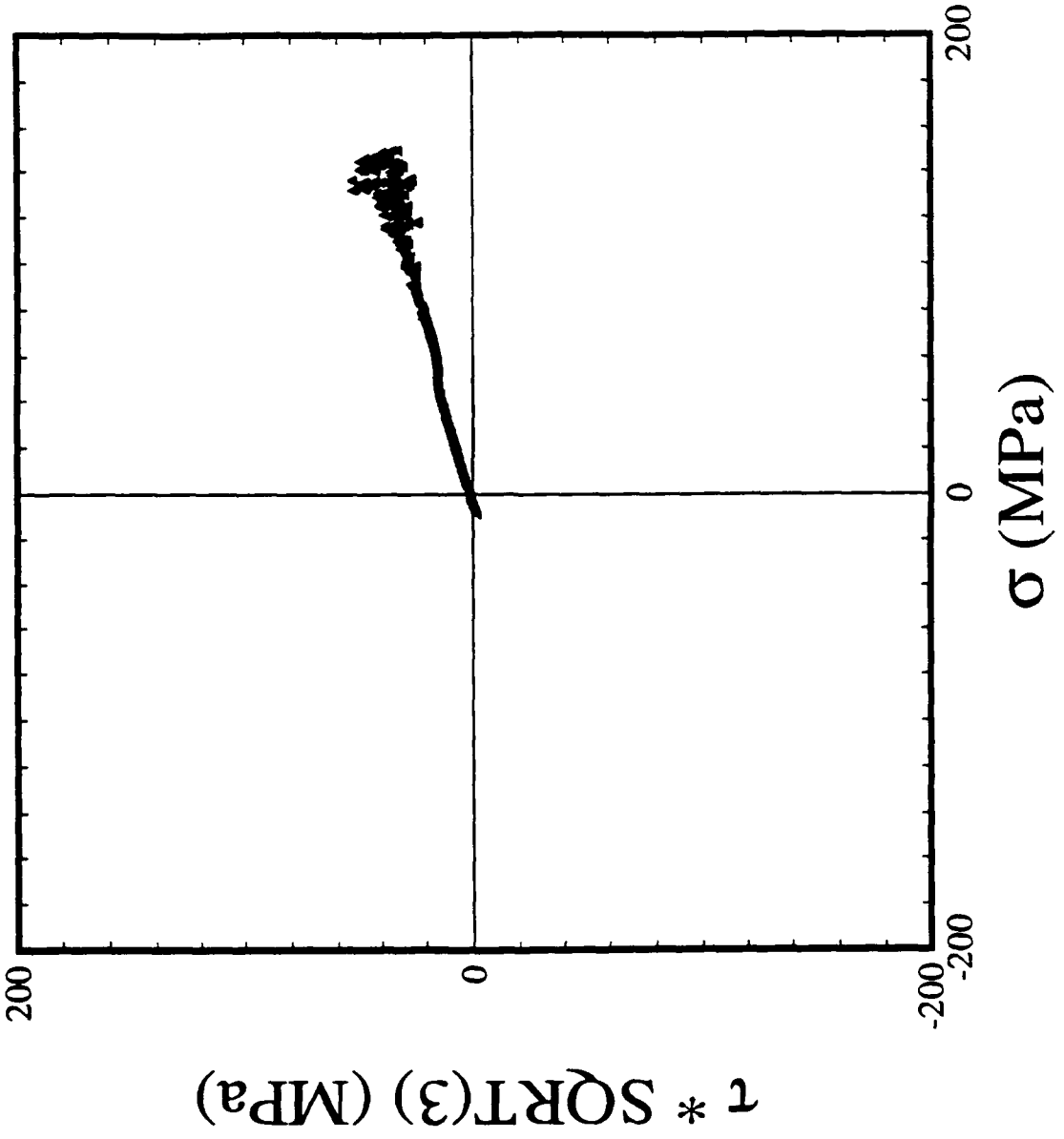

Figure 10b Recorded stress response from proportional straining path 34g2

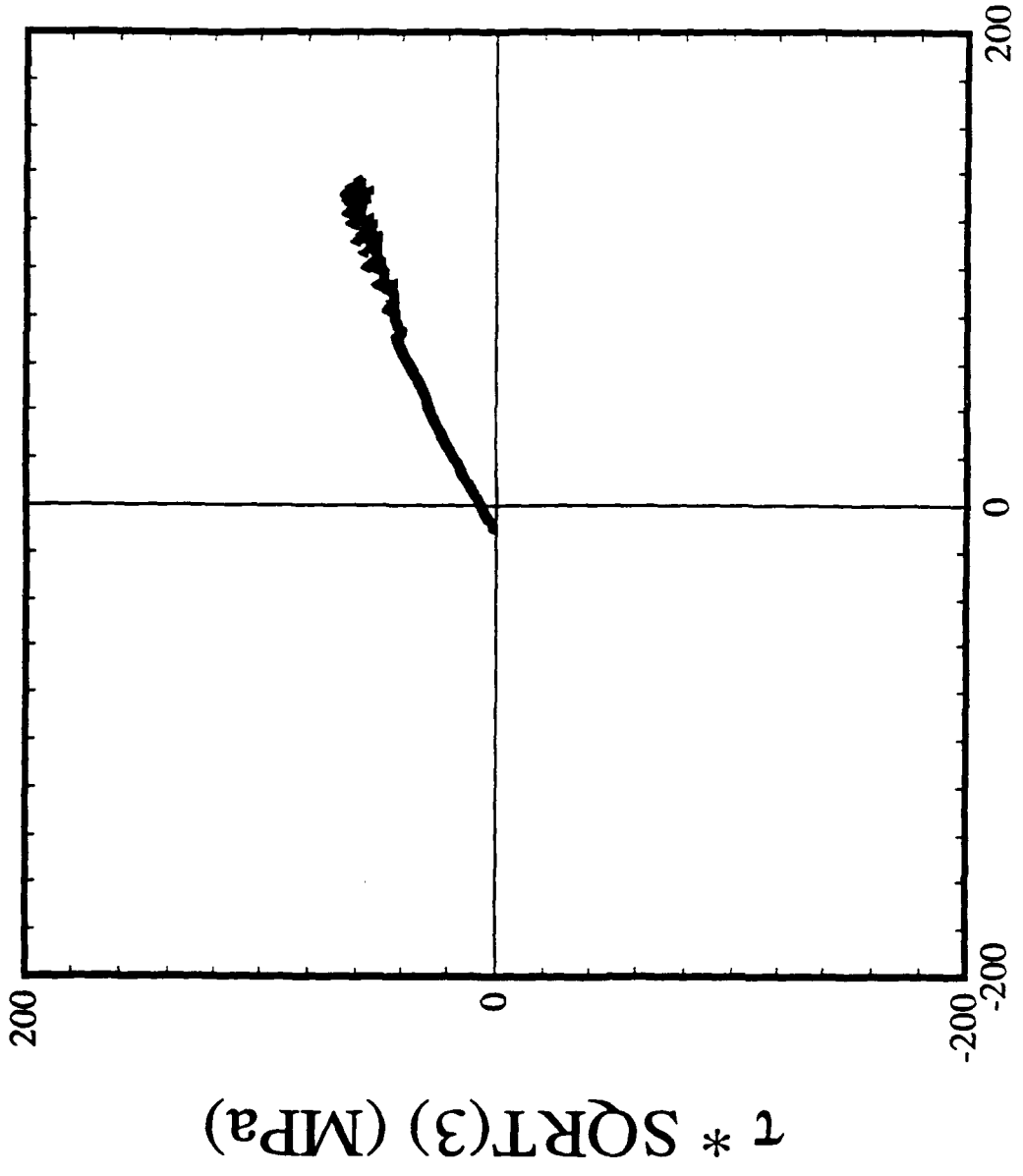

Figure 10c Recorded stress response from proportional straining path 34g3

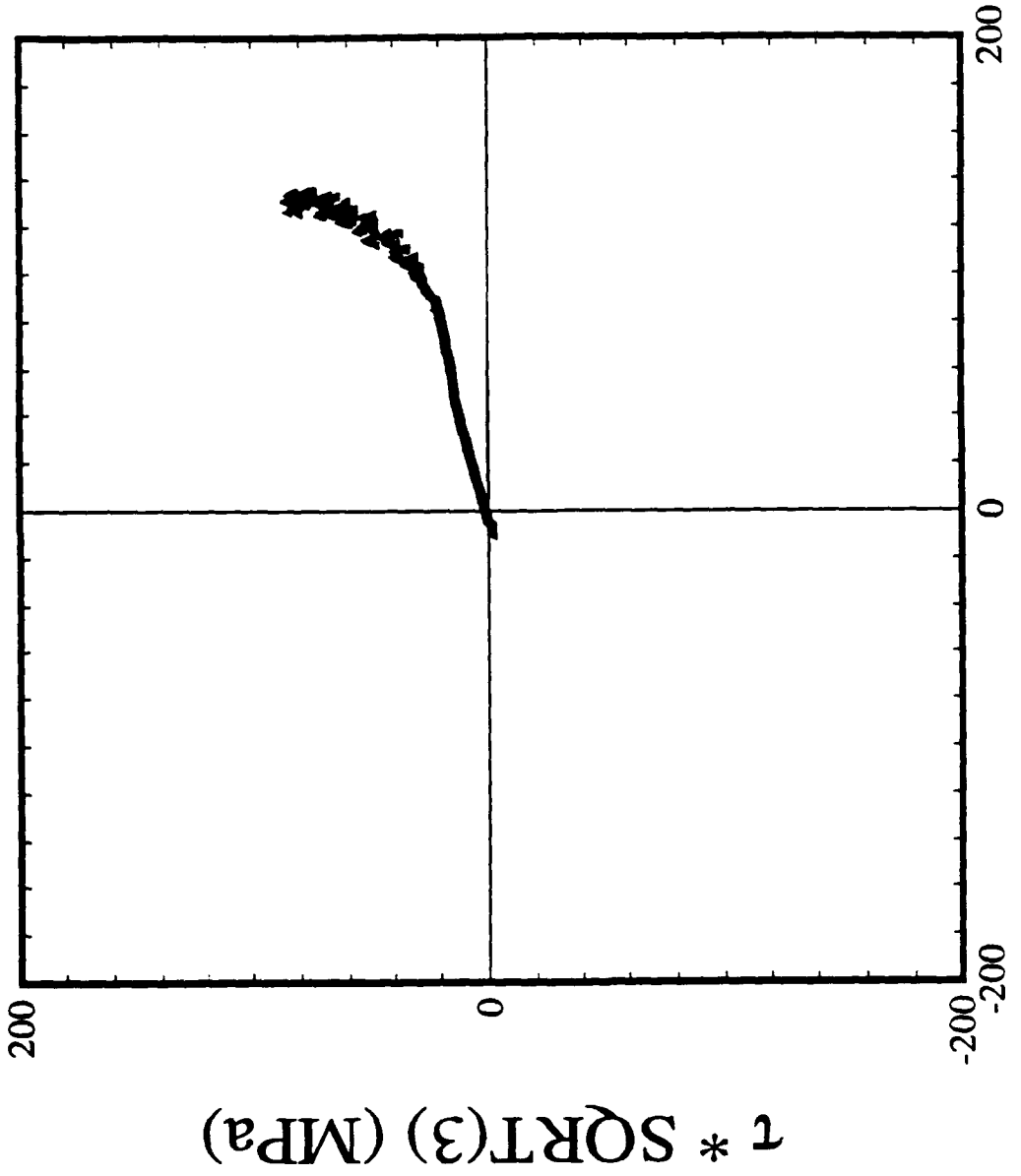

Figure 10d Recorded stress response from nonproportional straining path 34f3

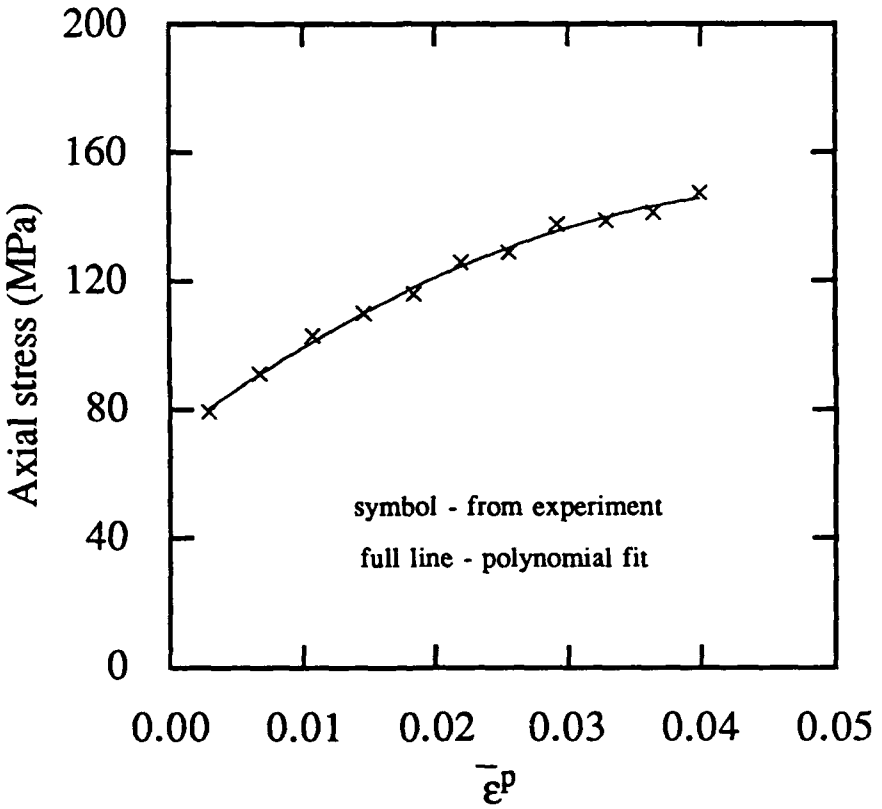

Figure 11a Axial stress versus generalized plastic strain from 34g2

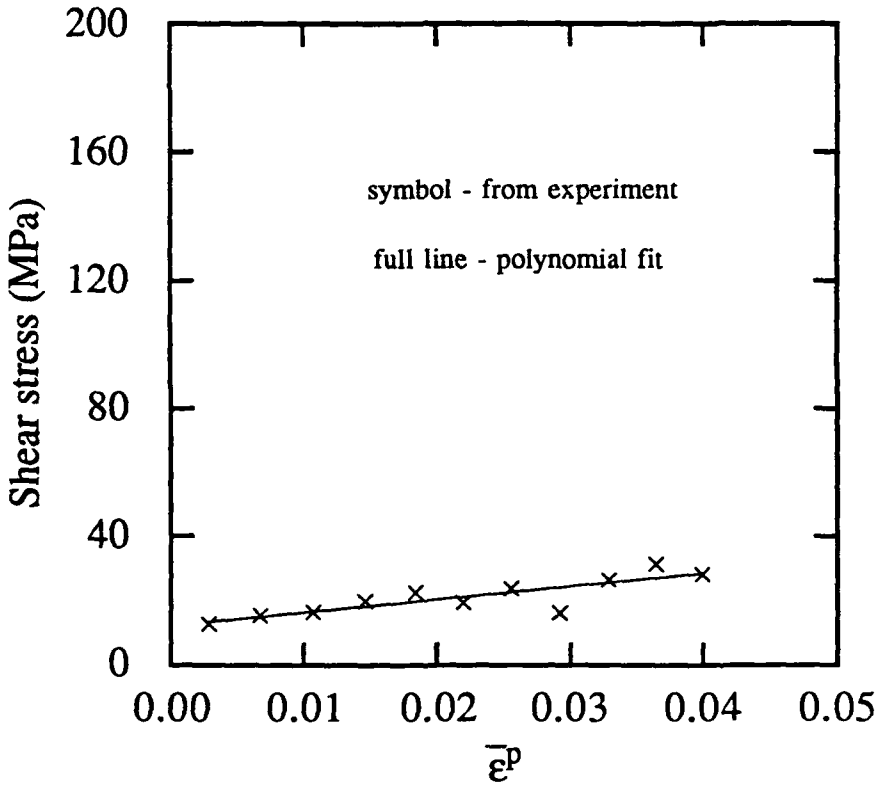

Figure 11b Shear stress versus generalized plastic strain from 34g2

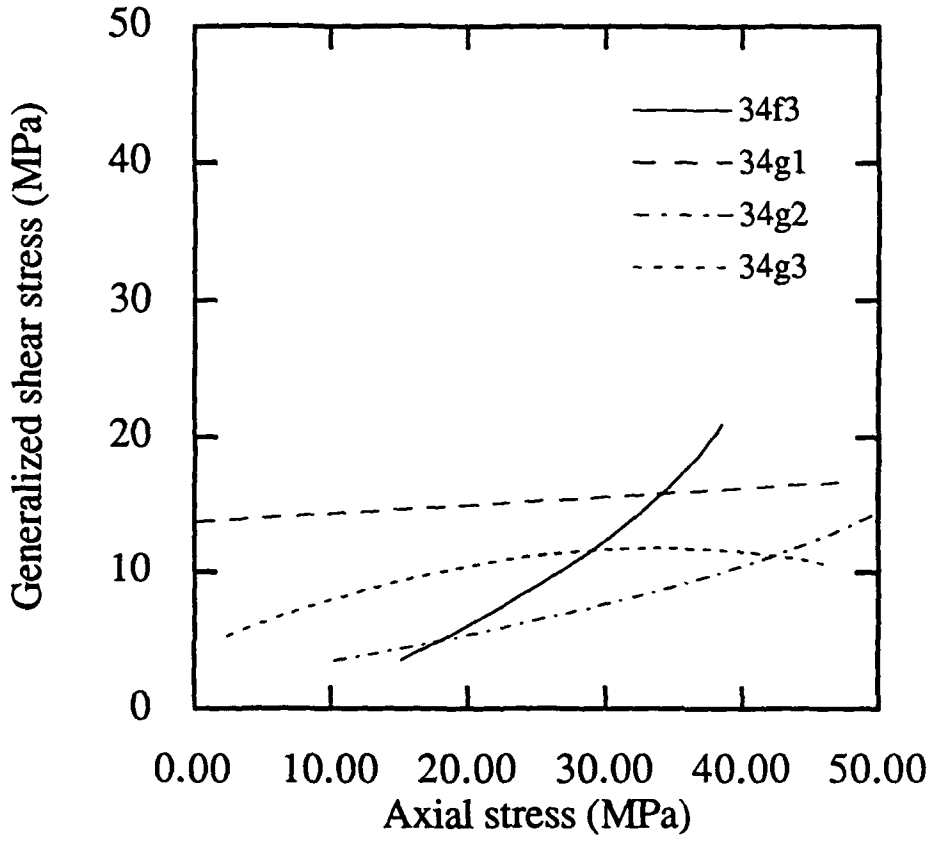

Figure 12 Trajectories of the centers of the circular yield loci

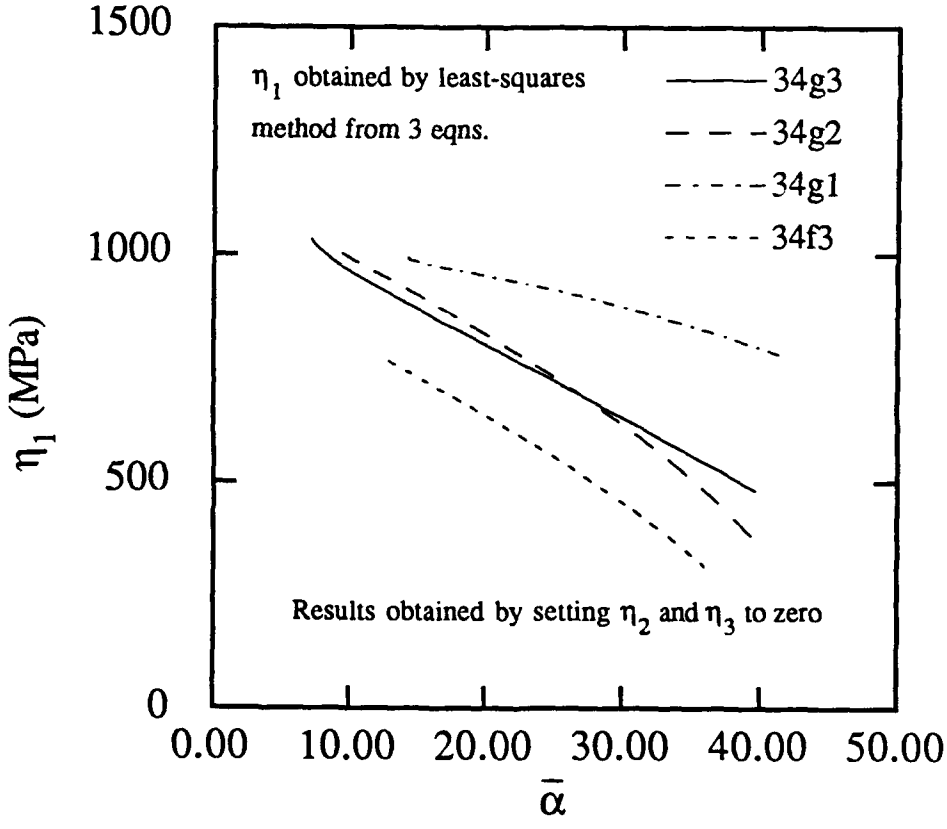

Figure 13 $\eta_1(\bar{\alpha})$ from all 4 straining paths

LIST OF PUBLICATIONS

1. "A Finite Element Method for an Incremental Viscoplasticity Theory Based on Overstress," T.-L. Sham and H.W. Chow, European Journal of Mechanics, A/Solids, Vol. 8, pp. 415-436, 1989.

2. "A Finite Strain Viscoplasticity Theory Based on Overstress," I. Nishiguchi, T.-L. Sham and E. Krempl, in "Advances in Plasticity 1989", Eds. A.S. Khan and M. Tokuda, Pergamon Press, N.Y., pp. 329-322, 1989.

3. "A Finite Deformation Theory of Viscoplasticity Based on Overstress, Part I: Constitutive Equations," I. Nishiguchi, T.-L. Sham and E. Krempl, Journal of Applied Mechanics, Vol. 57, pp. 548-552, 1990.

4. "A Finite Deformation Theory of Viscoplasticity Based on Overstress, Part II: Finite Element Implementation and Numerical Experiments," I. Nishiguchi, T.-L. Sham and E. Krempl, Journal of Applied Mechanics, Vol. 57, pp. 553-561, 1990.

5. "Some Basic Aspects of Elastic-Plastic Theory Involving Finite Strain," E.H. Lee, in "Constitutive Laws for Engineering Materials, Recent Advances and Industrial and Infrastructure Applications, Proceedings of the Third International Conference on Constitutive Laws for Engineering Materials: Theory and Applications, Tuscon, AZ, 1991;" Eds. C.S. Desai, E. Krempl, G. Frantziskonis and H. Saadatmanesh, ASME Press, NY, pp. 141-146, 1991.

6. "The Influence of Plastic-Strain-Induced Anisotropy, Modeled as Combined Isotropic-Kinematic Hardening, on the Stress Distributions Generated in the Finite Deformation of Ductile Metals," Y.S. Suh and E.H. Lee, in "Proceedings of the Korea Symposium on Science and Technology, Seoul, Korea, June 25-July 7, 1990", Korea Science and Technology Association, Seoul, pp. 1732-1736, 1990.

7. "The Influence of Plastic-Strain-Induced Anisotropy on Stress Distributions in the Finite Deformation of Ductile Metals," Y.S. Suh, Ph.D. Dissertation, Department of Mechanical Engineering, Aeronautical Engineering & Mechanics, Rensselaer Polytechnic Institute,

Troy, N.Y., 1990.

8. "Strain Induced Anisotropy during Nonproportional Straining Experiments and Modeling", S. Cheng, Ph.D. Dissertation, Department of Mechanical Engineering, Aeronautical Engineering & Mechanics, Rensselaer Polytechnic Institute, Troy, N.Y., 1991.

9. "Experimental Determination of Strain-Induced Anisotropy During Nonproportional Straining of an Al/Mg Alloy at Room Temperature," S. Cheng and E. Krempl, to appear in International Journal of Plasticity.

10. "Some Anomalies in the Structure of Elastic-Plastic Theory at Finite Strain," E.H. Lee, to appear in "Proc. Symposium on Nonlinear Effect in solids and Fluids to Honor Ronald S. Rivlin".

11. "Stress Analysis of Axisymmetric Extrusion in the Presence of Strain-Induced Anisotropy Modeled as Combined Isotropic-Kinematic Hardening," Y.S. Suh, A. Agah-Tehrani and K. Chung, to appear in Computer Methods in Applied Mechanics and Engineering.

12. "The Experimental Determination of the Stress Response of an Al/Mg Alloy to a Polygonal Strain Path after Three Levels of Prestraining," E. Krempl and S. Cheng, submitted to Acta Mechanica, 1992.

13. "The Stress Response and Yield Surface Changes During Nonproportional Straining of an Al/Mn Alloy at Room Temperature," E. Krempl and S. Cheng, draft manuscript complete.

14. "The Influence of Prestrain on the Stress Response of an Al/Mg Alloy to a Polygonal Strain Path," E. Krempl and S. Cheng, to appear in "Proc. Symposium of Mechanics, Mathematics and Materials", Army Symposium held at Plymouth, Ma., November, 1991.

15. "Development and Application of an Elastic-Plastic Constitutive Relation Involving Strain Induced Anisotropy Based on Nonproportional Straining Experiments," E.H. Lee, to appear in "Proc. Symposium of Mechanics, Mathematics and Materials", Army

Symposium held at Plymouth, Ma., November, 1991.

LIST OF PARTICIPATING SCIENTIFIC PERSONNEL

1. Erastus H. Lee, Rosalind and John J. Redfern, Jr., Professor of Engineering, Department of Mechanical Engineering, Aeronautical Engineering & Mechanics, Rensselaer Polytechnic Institute.
2. Erhard Krempl, Professor of Mechanics and Head, Department of Mechanical Engineering, Aeronautical Engineering & Mechanics, Rensselaer Polytechnic Institute.
3. Ting-Leung Sham, Associate Professor of Mechanical Engineering, Department of Mechanical Engineering, Aeronautical Engineering & Mechanics, Rensselaer Polytechnic Institute.
4. Yeong Sung Suh, Research Assistant, Department of Mechanical Engineering, Aeronautical Engineering & Mechanics, Rensselaer Polytechnic Institute, earned Ph.D. degree in 1990.
5. Shiyuan Cheng, Research Assistant, Department of Mechanical Engineering, Aeronautical Engineering & Mechanics, Rensselaer Polytechnic Institute, earned Ph.D. degree in 1991.